LANDSCAPE GEOMORPHIC ASSESSMENT IN ESTIMATING GROUNDWATER DISCHARGE INTO RIVERS IN HANNUKAINEN, NORTHERN FINLAND

Master's thesis

Vilma Lindgren

4.12.2018

Department of Geosciences and Geography

University of Helsinki

Tiedekunta – Fakultet – Faculty	Koulutusohjelma – Utbildningsprogram – Degree programme
Faculty of Science	Master's Programme in Geology and Geophysics

Tekijä – Författare – Author
Vilma Inkeri Lindgren

Työn nimi – Arbetets titel – Title
Landscape geomorphic assessment in estimating groundwater discharge into rivers in Hannukainen, Northern Finland

Työn laji – Arbetets art – Level	Aika – Datum – Month and year	Sivumäärä – Sidoantal – Number of pages
Master's thesis	12/2018	67

Tiivistelmä – Referat – Abstract

Three rivers in Hannukainen, in the Kolari municipality in Finland lie in the vicinity of an old mining site planned to be re-opened for mining activities. The rivers are known to have considerable inputs of groundwater (GW) due to earlier studies, and vulnerable natural salmonid populations. Two thermal infrared (TIR) datasets were used in this study from the Hannukainen area to find GW discharge locations and the landscape geomorphological factors affecting their occurrence; a TIR set collected in 2016 with an unmanned aerial vehicle (UAV) and a TIR set from 2012–2013 containing classified GW discharge site information.

The processing of the UAV data was described in detail and GW discharge sites were located manually in GIS. Discovered GW sites were classified into four categories: spring, diffuse seepage, relict channel and tributary confluence plume. Temperature profiles were created to examine the temperature changes along the rivers. The GW sites mostly caused only minor fluxes to the stream temperature, the main effect being on the landscape morphological features. Four landscape metrics were calculated from the GW discharge site TIR data 2012–2013 and open GIS data: channel sinuosity, gradient, terrain slope and entrenchment ratio (ER). The metrics were then statistically correlated with the GW discharge site locations. After the correlations ER was the only statistically significant metric indicating connections to the discharge site occurrences and counts. Low statistic model accuracy values and correlation coefficients were attained suggesting that a large part of the variance in the data remains unexplained by the metrics. There was a weak positive linear relationship between ER and the discharge site occurrences and counts, which means that more open valleys are more prone to having an increased amount of GW discharge sites. As the correlation is weak, a large part of the effects on the discharge amounts come likely from other riverine processes. The results partly agree and partly differ from the few studies that used similar metrics.

As used in this study the use of landscape metrics to predict the locations of GW discharge sites would be challenging and the reliability of results would be hard to ensure. More established methods for choosing, calculating and correlating the metrics are suggested. Also an inventory for metric values or value combinations representing the probable locations of GW discharge sites would be helpful in future studies.

Avainsanat – Nyckelord – Keywords
Groundwater discharge, thermal infrared methods, TIR, landscape metrics, spatial analysis, river morphology, Hannukainen, Kolari

Säilytyspaikka – Förvaringställe – Where deposited
HELDA – Digital Repository of the University of Helsinki

Muita tietoja – Övriga uppgifter – Additional information

Tiedekunta – Fakultet – Faculty	Koulutusohjelma – Utbildningsprogram – Degree programme
Matemaattis-luonnontieteellinen tiedekunta	Geologian ja geofysiikan maisteriohjelma

Tekijä – Författare – Author
Vilma Inkeri Lindgren

Työn nimi – Arbetets titel – Title
Landscape geomorphic assessment in estimating groundwater discharge into rivers in Hannukainen, Northern Finland

Työn laji – Arbetets art – Level	Aika – Datum – Month and year	Sivumäärä – Sidoantal – Number of pages
Pro gradu -tutkielma	12/2018	67

Tiivistelmä – Referat – Abstract

Hannukaisisissa, Suomen Kolarin kunnassa sijaitsee kolme jokea vanhan kaivosalueen läheisyydessä, jossa on suunnitteilla toiminnan uudelleenaloitus lähivuosina. Näissä joissa elää elinympäristön muutoksille herkkiä taimen- ja lohikalakantoja. Jokien vedestä merkittävä osuus koostuu aiempiin alueella tehtyihin tutkimuksiin perustuen jokiin purkautuvasta pohjavedestä, jonka purkupaikat voivat olla tärkeitä kaloille. Tässä tutkimuksessa käytettiin kahta alueelta kerättyä infrapunakuvausaineistoa pohjaveden purkupaikkojen ja niihin vaikuttavien maaston geomorfologisten muotojen yhteyksien löytämiseen: 2016 miehittämättömällä lennokilla (Unmanned Aerial Vehicle UAV) kerätty aineisto ja vuosilta 2012–2013 oleva aineisto alueelta löydetyistä pohjaveden purkupaikoista.

UAV-datan prosessointi kuvattiin yksityiskohtaisesti ja pohjaveden purkupaikat etsittiin manuaalisesti paikkatieto-ohjelmassa. Löydetyt purkupaikat luokiteltiin neljään luokkaan: lähde, laaja-alainen tihkupinta, vanha jokikanava ja sivujoen aiheuttama pluumi. Jokien lämpötilamuutosten tarkastelua varten tehtiin pitkittäiset profiilit. Pohjaveden purkupaikat aiheuttivat vain vähäisiä muutoksia lämpötiloihin, ja maaston geomorfologialla vaikutti olevan suurempi vaikutus. 2012–2013 purkupaikkadatasta ja avoimesta paikkatietodatasta laskettiin neljä maastoa kuvaavaa indikaattorimuuttujaa: kanavan mutkaisuus, gradientti, rinteen jyrkkyys ja entrenchment ratio (ER), joka on suhdeluku kanavan ja tulvalaakson leveyksistä. Muuttujat korreloitiin tilastollisesti pohjaveden purkupaikkojen sijaintien kanssa, joista vain ER:llä todettiin tilastollisesti merkittävä yhteys purkupaikkojen ilmenemisiin ja määriin. Tilastollinen tarkkuus oli huono käytetyssä mallissa, joten muuttujat eivät selitä purkupaikkoihin vaikuttavista tekijöistä paljoakaan. ER:n ja purkupaikkojen välillä oli heikko positiivinen korrelaatio, mikä tarkoittaa sitä, että mitä avoimempi jokilaakso kyseessä, sitä todennäköisemmin siellä esiintyy pohjaveden purkupaikkoja. Koska korrelaatio on heikko, luultavasti suurelta osin purkupaikkojen määrään vaikuttavat muut jokiprosessit. Tulokset ovat ainakin osittain yhteneviä samankaltaisissa indikaattorimuuttujatutkimuksissa.

Maastomuuttujien käyttäminen tulevissa tutkimuksissa samalla tavalla kuin tässä tutkimuksessa olisi hankalaa ja tulosten luotettavuutta vaikea arvioida. Muuttujien valintaan, laskemiseen ja korrelaatioon tarvittaisiin vakiintuneita metodeja. Lisäksi saatavilla olisi hyvä olla vertailukohtana käytettäviä muuttuja-arvoja, jotka edustaisivat todennäköisimpiä pohjaveden purkupaikkojen kohtia jokiympäristöissä.

Avainsanat – Nyckelord – Keywords
Pohjaveden purkautuminen, infrapunakuvausmetodit, jokimorfologia, paikkatietoanalyysi, Hannukainen, Kolari

Säilytyspaikka – Förvaringställe – Where deposited
HELDA – Helsingin yliopiston digitaalinen arkisto

Muita tietoja – Övriga uppgifter – Additional information

CONTENTS

1. INTRODUCTION

River water temperatures have a crucial impact on the animals and plants that reside there. Small temperature changes in the river water can have a significant effect on the occurrence and well-being of certain animal and plant species (e.g. Ebersole et al. 2003a, Monk et al. 2013, Dugdale et al. 2015). Some salmonids are known to be very sensitive to high temperatures in their river habitats and the fish prefer colder water patches in the river to avoid heat stress in the summer. These cold water patches named hereafter as thermal refuges are formed when the stream receives colder water from groundwater discharge from for example the streambed or a cool tributary.

Summer river temperatures have been observed to rise in North America, Europe and Africa and climate change will likely warm the salmonid rivers even more in the future (Jonsson and Jonsson 2009). Therefore, the role of thermal refuge habitats in rivers for temperature sensitive species will increase in the future (Monk et al. 2013, Dugdale et al. 2015). Also, the importance of understanding the mechanisms affecting the occurrence of these refuges will keep growing. Predicting the locations of existing cold water refuges enables conservation efforts to concentrate on the right locations of a river for best results (Torgensen et al. 2012). With conservation, the restoration of floodplain connectivity and riparian vegetation is attempted so that natural thermal heterogeneity in the stream could restart.

Three rivers in Hannukainen study area located in Kolari municipality in Northern Finland are known for rich populations of natural salmon and sea trout (Vähä et al. 2014). The rivers Äkäsjoki, Kuerjoki and Valkeajoki are a part of Tornionjoki watershed, the largest watershed in the Baltic Sea. An old mine site resides in Hannukainen in the close vicinity of these rivers as well, where iron, copper and gold were mined from the 1970's to 1990. In 2005, Northland mines Ltd began mine prospecting in the area again, and large-scale environmental investigations and reports were performed to restart mining (Hannukainen mining 2017). However, in 2014 Hannukainen mining Ltd bought the rights for the area and continued mining development activities. The new company is planning to start building infrastructure in the area in 2019 and start open pit mining in 2022.

Due to the ore potential, several studies associated with the iron-copper-gold ore deposits have been conducted in the Rautuvaara and Hannukainen area (e.g. Hiltunen 1982, Niiranen et al. 2007). The area is also located in the Lapland ice-divide zone and therefore it has been studied thoroughly throughout decades for its stratigraphic key sites describing the general Quaternary stratigraphy of Finland (e.g. Kujansuu 1967, Hirvas 1991, Salonen et al. 2014a). More recently the interactions between groundwater (GW) and surface water (SW) have been studied in the area for better understanding of the extent of the water exchange and the possible effects of mining activities to the rivers (Salonen et al. 2014b, Rautio et al. 2017).

Thermal methods utilizing TIR remote sensing and geographical information systems (GIS) have been proven to be effective in studying the occurrence of GW discharge in stream environments (Torgensen et al. 1999, 2001, Monk et al. 2013, Dugdale et al. 2015). Thermal infrared (TIR) imaging is conducted either with a helicopter or an unmanned aerial vehicle (UAV). Recent studies utilize high resolution TIR imaging and the spatial analysis of landscape metrics calculated from geomorphological features associated with the rivers to examine the processes that affect the spatial distribution of the GW discharge into the rivers (Monk et al. 2013, Dugdale et al. 2013, 2015, Wawrzyniak et al. 2016). This includes calculating the landscape metrics from geomorphological features associated with the rivers and linking the metrics to the occurrence of GW discharge sites in GIS to find out which of the metrics are the most influential. The rivers in Hannukainen are shallow and well mixed, there is no excessive vegetation blocking the view from above and a sufficient temperature difference between SW and GW exists, providing an excellent place for a TIR study.

Materials used in this study include TIR data collected in 2012–2013 with recognized groundwater discharge sites in the Hannukainen region (published in Rautio et al. 2017) and additional TIR data collected in 2016 by UAV. The term GW discharge site includes all cold water patches next to or in the rivers and the suitability of the discharge sites as thermal refuges for fish is discussed later. Firstly, I describe methods for TIR data collecting and processing and classifying GW discharge sites for the 2016 UAV Hannukainen data. River geomorphological features that can indicate GW discharge into the rivers in Hannukainen

are identified and measured with GIS and statistical software using the existing 2012–2013 GW discharge site and open GIS data. Secondly, the GW discharge to the rivers is examined from both datasets, and the connections between the landscape metrics, river morphology and the GW discharge are discussed. Finally, the applicability of the used methods for these processes is assessed.

The aim of this study is to find landscape metrics that can be used to recognize GW discharge sites into the studied streams. Also, classification of GW discharge sites is performed and the processes affecting the GW discharge are examined. The study aims to answer the following questions:

1. Is it possible to predict the occurrences of GW discharge sites with landscape metrics?
2. Could the landscape metrics methods used in this study be utilized in later studies to predict GW site locations?
3. What processes affect the GW discharge in the study area?

It would also be useful to have ready landscape metrics methods to be used in later studies for discovering GW discharge sites or thermal refuges from areas with no available TIR data. The findings of this study could also give important insight about the local connections of the rivers in Hannukainen and the GW reserves regarding the future mining activities or salmonid studies.

2. STUDY AREA

The study site is located in Hannukainen, Kolari, Northern Finland (Figure 1). Three rivers were examined in the study: Äkäsjoki, Kuerjoki and Valkeajoki. Kuerjoki and Valkeajoki are tributaries of Äkäsjoki, which is a tributary of Muonionjoki and eventually Tornionjoki. Äkäsjoki is 51 km long and has a total catchment area of 649 km² including the catchments of Kuerjoki and Valkeajoki. Kuerjoki is 22 km long and has a 162 km² catchment area. Valkeajoki has a 53 km² catchment area and is 12.3 km long and the width of the river varies between 1 and 12 m. The whole Valkeajoki catchment area and river belong to the study area. Two subcatchments of Äkäsjoki are included in the study area: Hannukainen and the Äkäsjoki river mouth. Kuerjoki is represented by its subcatchment nearest to Äkäsjoki (Kuerjoki area). The catchment areas are represented in Figure 2. The Hannukainen subcatchment has an area of 52 km² and the Äkäsjoki subcatchment 57 km², totaling an area of 109 km². The length of the studied part of the Äkäsjoki river is in total 15.5 km long with the river width varying between 10 and 38 m (Table 1). The Kuerjoki subcatchment has an area of 61 km² and the studied part of the river is 7.5 km long with widths between 6 and 28 m (HERTTA database).

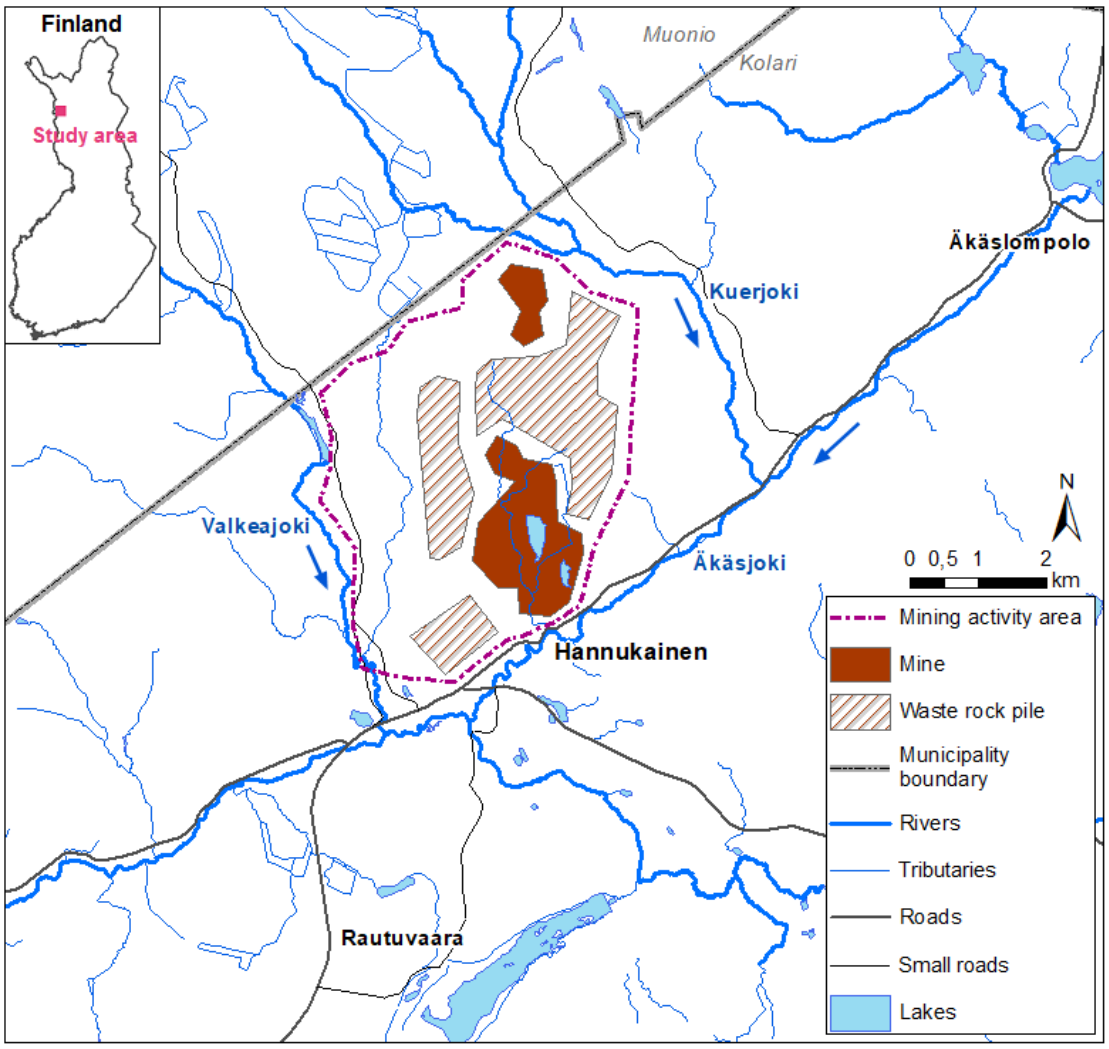

Figure 1. The Hannukainen study area and the planned mining activity area. Kuervitikko deposit is the smaller and Laurinoja deposit is the larger planned mine area. (Map of Finland and base map database, ©National Land survey of Finland (NLS) 2010; river network database, ©Finnish Environmental Institute (SYKE) 2015; mining site area from Hannukainen mining 2017.)

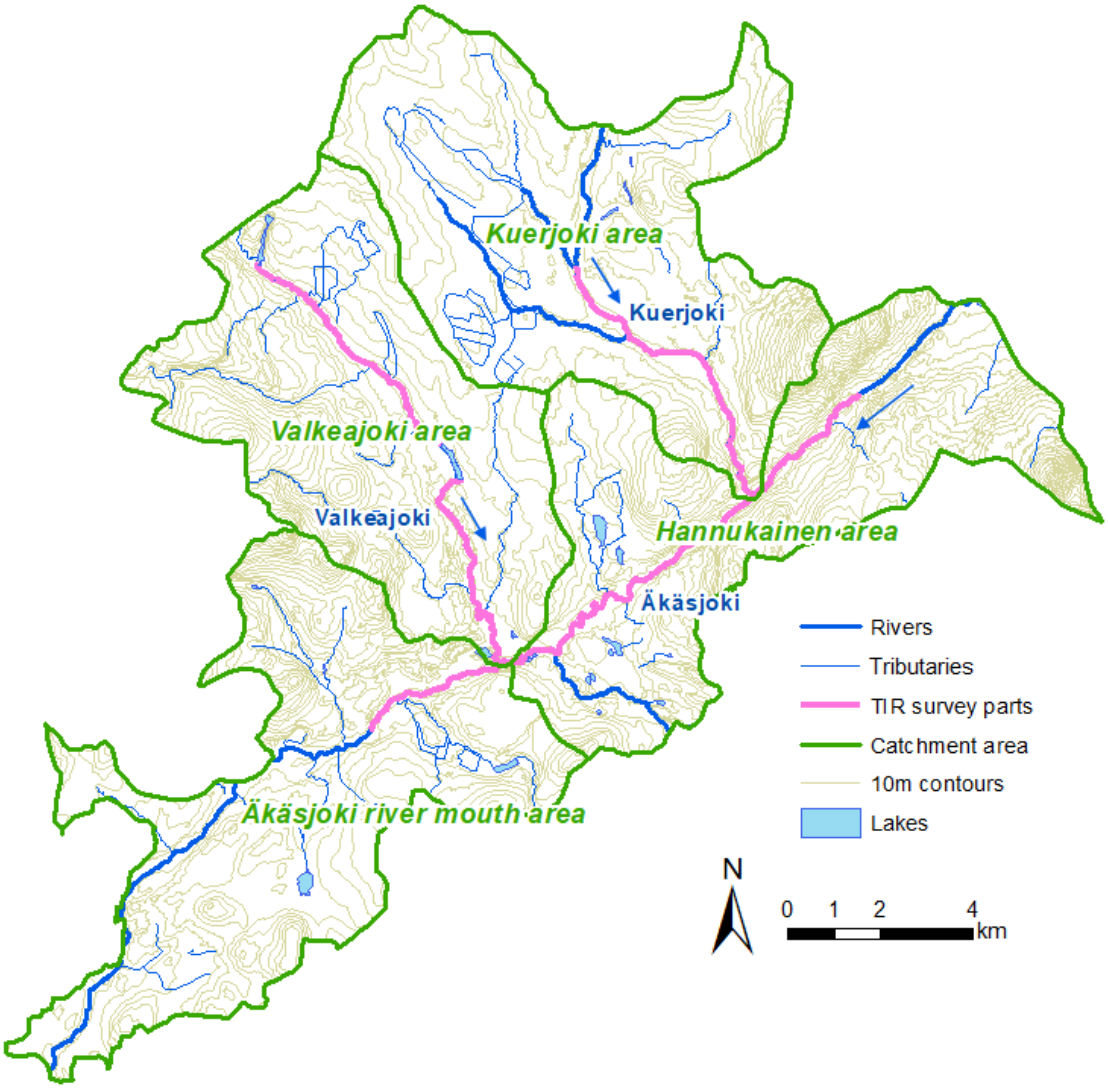

Figure 2. Catchment areas and the 2012–2013 TIR survey river parts (base map database, ©NLS 2010; river network database, ©SYKE 2015).

Mean discharge rates of the studied rivers are in Table 1. The rates vary greatly depending on the season: in the spring in May the snow melts and the discharge rates are at maximum, even tenfold compared to the mean rates of the year. The mean discharge of Kuerjoki is about one third and the mean discharge of Valkeajoki about one tenth of the mean discharge of Äkäsjoki in the Hannukainen area. A mean discharge rate of 1.1 m^3/s for Valkeajoki was measured in the field 1.2 km from the river mouth, and it is about twice the size of the yearly mean discharge in the river mouth.

Table 1. River info in the extent of the study area. Discharge rates based on 1962–2010 data from a catchment model system maintained by the Finnish Environmental Institute (2012). MQ = mean discharge, MNQ = mean minimum discharge, MHQ = mean maximum discharge.

	Subcatchment area (km²)	Length (m)	Width range (m)	MQ (m³/s)	MNQ (m³/s)	MHQ (m³/s)
Äkäsjoki	109	14.5	10–38	4.8	1.9	55
Kuerjoki	61	7.5	6–28	1.6	0.4	21
Valkeajoki	53	12.3	1–12	0.5	0.1	6.8

Tourism, forestry, agriculture and reindeer herding are the most important livelihoods of the Kolari region people. Next to Äkäslompolo village is the Ylläs fell which offers winter sports activities and is a significant tourism attraction in the area (Pöyry Finland Ltd 2010). Fishing is a popular leisure activity in the rivers, as there are salmon, trout and other fish. Tornio River is the largest watershed in the Baltic Sea with significant natural salmon and sea trout populations also in a global scale. (Vähä et al. 2014) The land cover in the area is mostly mixed forest, woodlands or shrubs and peatbogs (Figure 3). The Äkäslompolo village in the eastern part of the map is shown as sport and leisure facilities and industrial or commercial units. Part of the Ylläs fell in the easternmost part of the map is shown as bare rock.

There is an old mine site in Hannukainen. Iron, copper and gold were mined by Rautaruukki from Rautuvaara and Hannukainen from the 1970's to 1990 (Hannukainen mining 2017). Waste rock areas of the old mine are shown as dump sites between Kuerjoki and Valkeajoki along with two old mine pits filled with water. Hannukainen mining Ltd is planning to start building infrastructure in the area in 2019 and to start open pit mining in Laurinoja deposit in 2022 and the Kuervitikko deposit some years later.

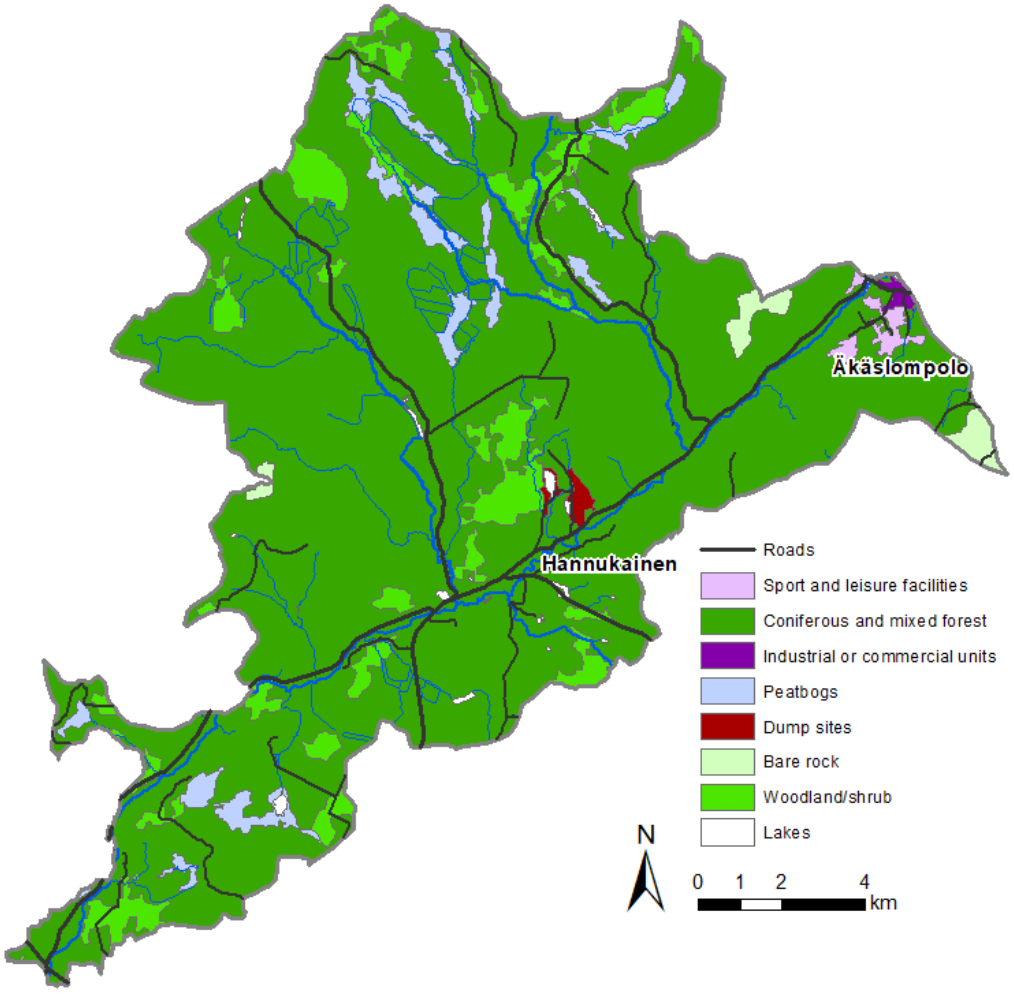

Figure 3. Land use of the study area according to CORINE classes (base map database, ©NLS 2010; CORINE classification, ©SYKE 2012).

The nearest point of available meteorogical data is Muonio where data has been collected from 1981 to 2010, located 50 km north of Hannukainen, where the annual average temperature is -1.0°C and for the summer months (Jun-Aug) 12°C. Annual average precipitation is 521mm of which 208mm precipitates in the summer months (Pirinen et al. 2012).

2.1 Geological setting

There are classified GW areas belonging to classes II and III in the study area (Figure 4). In this study, the old classification based on water supply demands is used as the reclassification

of GW aquifers is still ongoing. Class I aquifers are described as important for water supply, class II as suitable for water supply and class III as other GW areas (HERTTA database).

The GW flow patterns in the planned mining site between Valkeajoki and Kuerjoki are complex and have been studied by Salonen et al. 2014b and Rautio et al. 2017. According to Salonen et al. 2014b the GW reserves are in many levels among the permeable and impermeable units in the aquifers. Bedrock ridges divide the area into three basins that channel the GW flow towards Äkäsjoki, Valkeajoki and Kuerjoki (Figure 4). At least part of the water in the studied rivers consists of GW, especially in Kuerjoki and Valkeajoki where GW is the dominant water source (Salonen et al. 2014b).

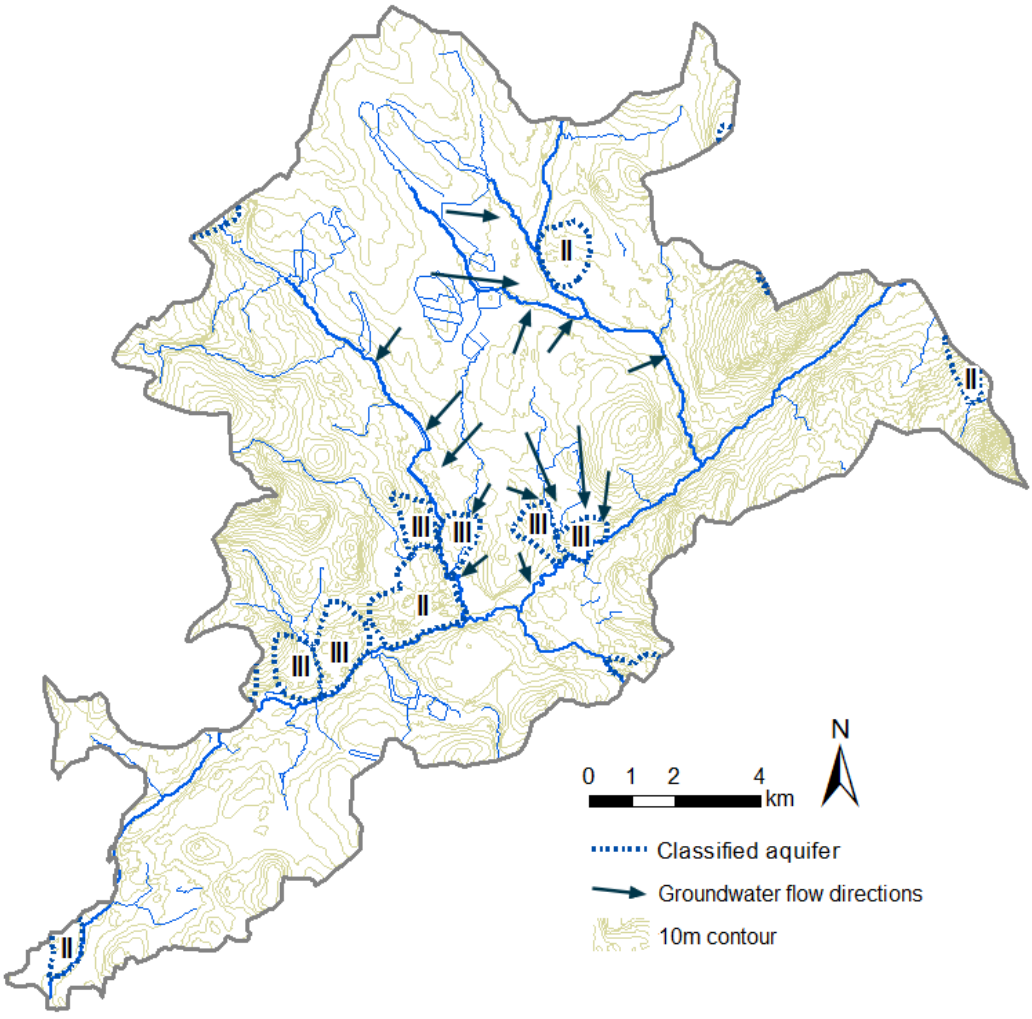

Figure 4. Classified aquifers from HERTTA database and groundwater flow directions in the study area according to Salonen et al. 2014b (base map database, ©NLS 2010; river network database, ©SYKE 2015).

2.1.1 Bedrock

Hannukainen resides in the Central Lapland greenstone belt. The bedrock in the area consists of granite, intrusive monzonite and diorite in the western side and quartzite and mica gneiss in the eastern side (Figure 5). A complex system of thrusts and faults associated with the contact zone between Savukoski Group supracrustal sequence and the monzonite-diorite intrusions forms the Kolari shear zone. Almost all of the iron oxide-copper-gold (IOCG) deposits in the area are associated with skarns that formed in the intrusion events. The skarns compose mostly of clinopyroxene and amphibole dominated rocks. The IOCG ore deposits comprise of massive to silicate-banded magnetite-rich lenses (ironstones) (Hiltunen 1982, Niiranen et al. 2007). A large Hannukainen iron ore deposit was found in 1974 by Rautaruukki and extensive bedrock drilling has been conducted in the area (Hiltunen 1982). Future mining plans in Hannukainen are focused on the Laurinoja and Kuervitikko Fe-Cu-Au deposits (Figure 1, Hannukainen mining 2017).

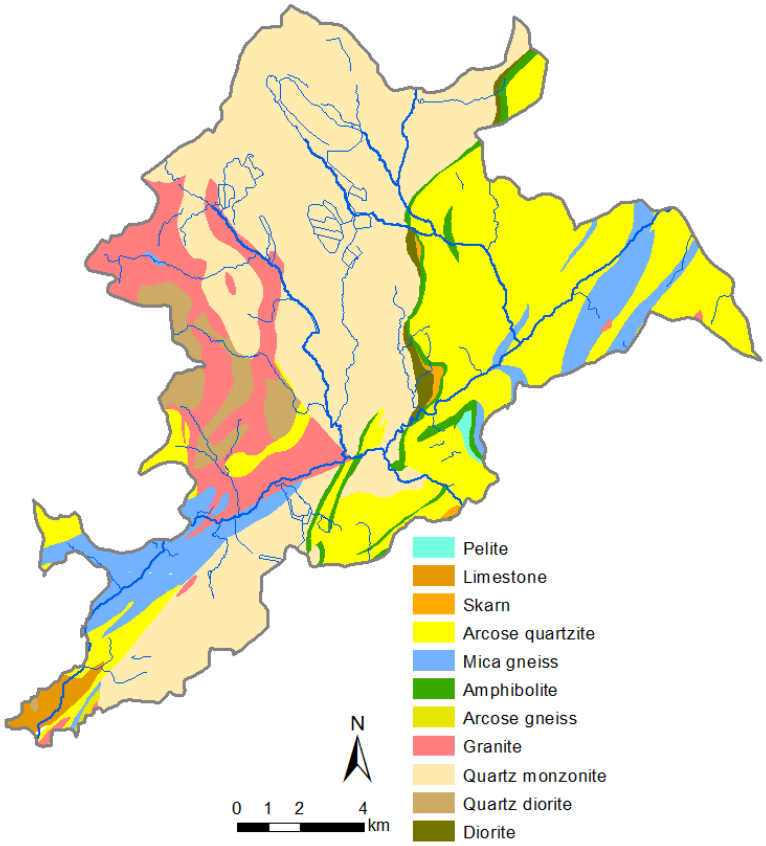

Figure 5. Bedrock map of the study area (bedrock of Finland 1:100 000, ©Geological Survey of Finland 2014; river network database, ©SYKE 2015).

2.1.2 Surface deposits

Finnish Lapland has a complex Quaternary glaciation history, which can be observed from many well preserved Middle and Late Pleistocene organic and glacial sediments. Hannukainen belongs to the ice-divide zone of the last glaciation. The zone is characterized by a thick preglacial weathering crust and a relatively thin till cover resulting from very weak glacial erosion (Kujansuu 1967). The Rautuvaara open pit area near Hannukainen is a key stratigraphic site and it has been among other sites a valuable resource in explaining the general Quaternary stratigraphy of Finland (Hirvas 1991). In Finnish Lapland six significant till beds occur with interbedded silt, sand and organic sediments according to Hirvas (1991). The Rautuvaara section has five of the oldest beds. Till beds I–III are thought to represent the Weichselian Stage, till bed IV the Saalian glaciation and till beds V and VI glacial stages before the Holsteinian interglacial. However, newer studies have suggested that all of the till beds were deposited during the Weichselian Stage. Also, two time intervals of ice-free conditions in Western Lapland have likely occurred during the Mid-Weichselian (Salonen et al. 2014a and Lunkka et al. 2015).

A 1:200 000 surface geology map is the most specific quaternary deposit map of the Hannukainen area available (Figure 6). Till is the most common surface deposit, and the river valleys are dominated by sands and gravels. Near the mouth of Kuerjoki the river is flowing partly in steep bedrock canyons. Peat deposits are common especially at Kuerjoki and partly Valkeajoki headwaters. Bedrock outcrops are not common in the area but due to the thin surface deposit layer near-surface bedrock is quite common. In the eastern part of the area there are some fine-grained silts where the Äkäslompolo Lake resides and some block fields associated with the Ylläs fells.

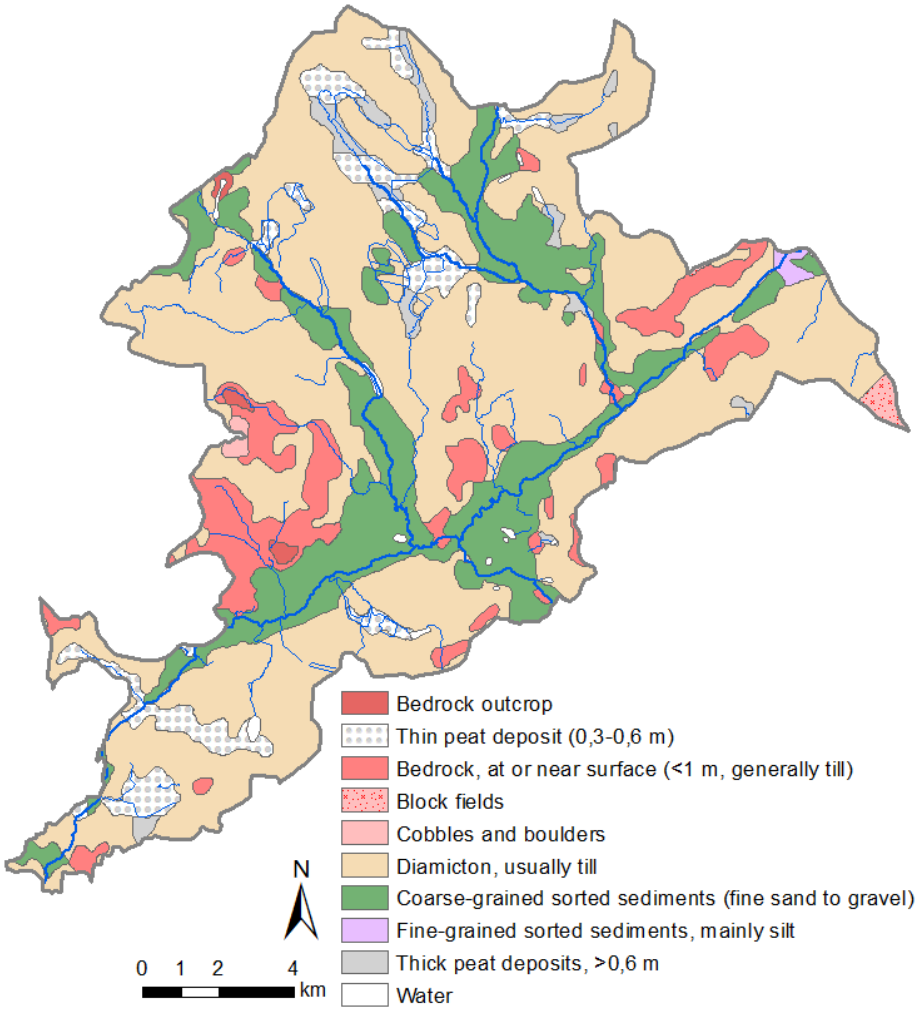

Figure 6. Surface deposits of the study area (superficial deposits of Finland 1:200 000, ©Geological Survey of Finland 2012; river network database, ©SYKE 2015).

There are, however, variable Quaternary deposits below the topmost till unit. According to Salonen et al. (2014b) the thickness of the Quaternary sediment bed in the area varies between 0 to 102 meters with a median thickness of 18 meters. Three hydrostratigraphical units or aquifers were identified in the planned mining area with low-permeability aquitards in between along with a system of perched GW bodies. The aquifers consist of permeable fluvial and deltaic sands and gravels and the aquitards comprise of tills and finer materials.

3. TIR METHODS IN DEFINING STREAM GROUNDWATER DISCHARGE

TIR methods provide a faster way to identify gaining or losing reaches in streams compared to conventional, direct measurement techniques, and also in difficult terrain (Rosenberry and Labaugh 2008). TIR sensors detect thermal energy only in the water surface, therefore methods utilizing the technology can only be used where the water column is thoroughly mixed (Monk et al. 2013). In stream environments where turbulent flow prevails, thermal stratification is usually not a problem. The best conditions for TIR studies in Finland are from July to August when the temperature difference between ground and river water is at maximum (Torgensen et al. 2001, Rautio et al. 2015).

UAVs are the newest addition to thermal imaging options. They operate autonomously, fly low and slowly and are cost-effective at a detailed and areally limited scale by eliminating the need for a helicopter to conduct the study flights (Faye et al. 2016). The flight paths can be planned ahead with a computer/tablet program. UAV can be equipped with both an RGB and a thermal imaging cameras, GPS and a data connection for inflight monitoring and control. Reference water temperature measurements are collected usually with probes or loggers during the flights to validate the TIR water temperatures (e.g. Torgensen et al. 1999 and Dugdale et al. 2013). Possible distortions in the TIR data can be recognized and fixed by recording meteorological conditions such as global solar radiation and air temperature during the flights (Faye et al. 2016). Also, to improve the scale, orientation and position of orthomosaics created from the RGB photos, black canvas sheets can be placed on the ground before the flights to serve as ground control points.

TIR and ortho imagery acquired for a study require thorough processing to find GW discharge sites. Comparison of ortho and thermal imagery was used by Wawrzyniak et al. (2016) to prevent recognition of cold-appearing shaded terrestrial areas as GW discharge sites. Both manual methods in GIS (Monk et al. 2013, Wawrzyniak et al. 2016) or MATLAB (Dugdale et al. 2013, 2015) and automated methods (Wawrzyniak et al. 2016) have been used in detecting the GW discharge sites. Areas that match the temperature and area

requirements for a GW discharge site are listed and classified according to their form and geomorphological features. Then river landscape features are chosen for inspecting possible correlations with the discharge sites. These features include for example drainage network, basin topography/geomorphology, watershed geology, basin land cover and soil and bedrock geology (Monk et al. 2013, Dugdale et al. 2015). If sufficient data resolutions are available of the relevant features, landscape metrics are calculated from the features, and the metrics are then correlated with the occurrence of the GW discharge sites with statistical software.

3.1 Groundwater discharge site definitions and terminology

TIR methods are effective only if the temperature difference between SW and GW is notable enough. A cold anomaly with a 0.5 to 3 °C difference to the main river stem ambient streamflow has been used as a marker of a GW discharge site in many studies (Ebersole et al. 2003a, Dugdale et al. 2013 & 2015, Rautio et al. 2015, Wawrzyniak et al. 2016). Also a minimum area requirement of 0.5 to 2.25 m² for a GW discharge site has been used by e.g. Ebersole et al. 2003a, Dugdale et al. 2015 and Wawrzyniak et al. 2016. In this study, a GW discharge site has a minimum of 0.5 °C difference compared to the ambient streamflow similar to e.g. Dugdale et al. 2013, 2015 and Wawrzyniak et al. 2016 and a minimum size of about 0.5 m² similar to Ebersole et al. 2003a.

GW discharge site is the term used to describe a cold anomaly in this study, but other terms are also used such as thermal refuge (Dugdale et al. 2013, 2015, Monk et al. 2013, Torgensen et al. 2012), cold water patch (Ebersole et al. 2003a, 2003b, Wawrzyniak et al. 2016), GW discharge area (Rautio et al. 2015) and GW discharge zone/site (Korkka-Niemi et al. 2012). As mentioned before, thermal refuges are cold water areas that provide shelter for aquatic species (e.g. Ebersole et al. 2003a) and the GW discharge sites examined in this study include areas that are not in the river channel so only a part of the studied discharge sites could be potential thermal refuges.

4. MATERIALS AND METHODS

4.1 TIR and groundwater discharge site data collected in 2012–2013

This study utilizes existing TIR and GW discharge site data from the Hannukainen area collected in July 2012 and August 2013 in a GW – SW interaction study by Rautio et al. (2017). A more detailed method description is available in Rautio et al. 2017. The acquired data includes ortho and TIR video files from Äkäsjoki, Kuerjoki and Valkeajoki which were used also as reference and comparison with the UAV data. However, the most important part of the data consisted of excel tables of identified GW discharge sites in the area with their coordinates, temperatures and classes (Figure 7). The tables were imported into GIS as GW discharge site point data to be used in spatial analyses with the landscape metrics (see 4.3 Landscape metrics).

Details of the 2012–2013 GW discharge site data are in Table 2. Valkeajoki had the highest GW discharge site density with 15.1 sites per km. Kuerjoki had a density of 11.1 and Äkäsjoki 5.7 per km. Rautio et al. 2017 defined a thermal anomaly as an area over 0.5 m^2 with a temperature difference of at least 2–3 °C compared to the ambient air temperature during the TIR surveys.

Table 2. Details of the 2012–2013 TIR survey data used in this study (Rautio et al. unpublished).

River	Year collected	GW discharge site count	Length of studied section km	GW discharge site density km-1
Äkäsjoki	2012	83	14.5	5.7
Kuerjoki	2012, 2013	83	7.5	11.1
Valkeajoki	2012, 2013	186	12.3	15.1

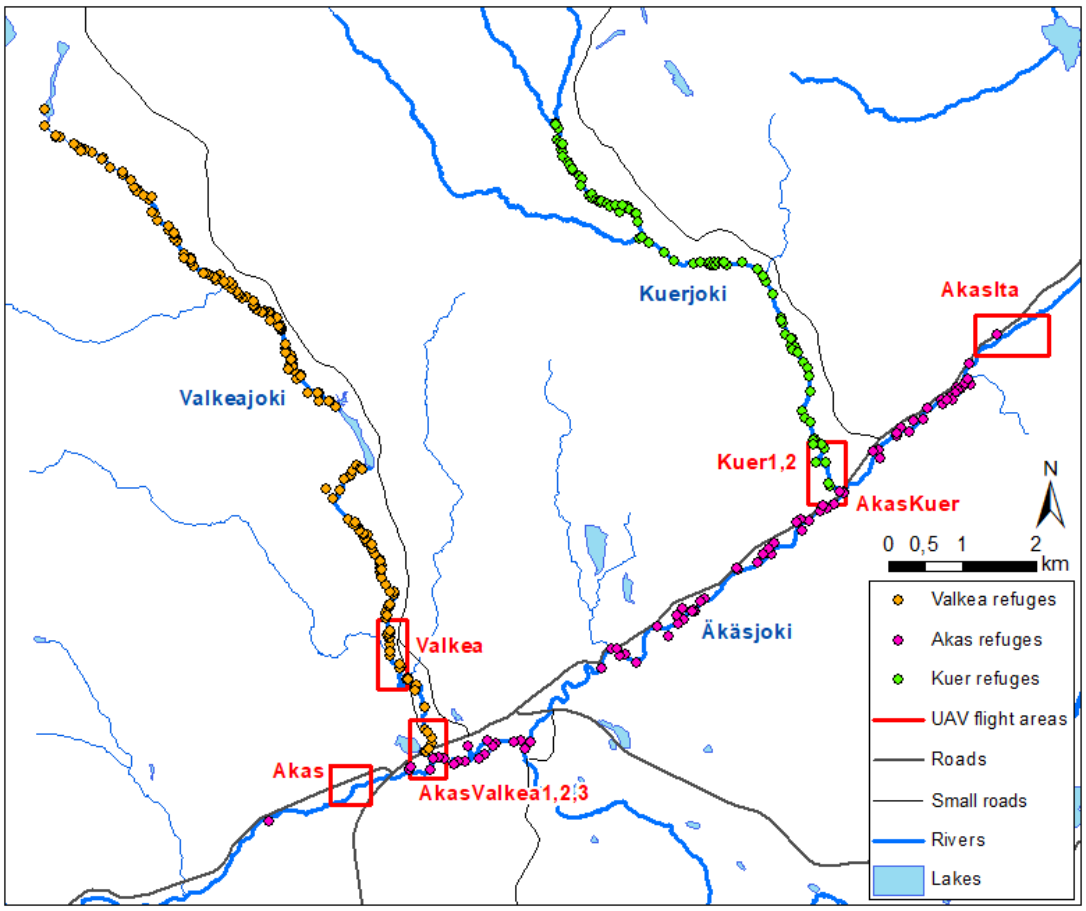

Figure 7. Locations of the UAV survey and the 2012-2013 groundwater discharge site data (Rautio et al. unpublished, river network database, ©SYKE 2015).

4.2 TIR survey in 2016

4.2.1 UAV survey

A field campaign to Hannukainen to collect data was made in August 2016 during the low flow season. A Matrice 100 quadcopter UAV was used for collecting the TIR and ortho image data (Figure 8) and a sediment temperature probe (Therma Plus) was used for reference temperature measurements at the surveyed river sections along rivers Valkeajoki, Äkäsjoki and Kuerjoki (Table 3, Figure 7). The UAV was equipped with a DJI Zenmuse X3 gimbal and a FLIR TAU2 640 thermal imaging camera (640 x 512 pixels) integrated with a TeAx ThermalCapture module and a DJI FC350 RGB camera unit with a resolution of 4000 x 3000 pixels. The flight altitude was set to 100 meters above the ground surface so that the

actual flight altitude varied between 270–340 meters above the sea level. Each flight yielded 3000–5700 TIR images and 80–130 RGB images. Mean pixel resolutions of 4.6 and 13.4 cm were attained for the RGB and TIR datasets, respectively.

Figure 8. The Matrice UAV and control equipment used in the imaging. (©Vilma Lindgren)

Flight paths for the UAV were planned with an IPad tablet with Map Pilot application (©Maps Made Easy). Every time at a new flight location the UAV compass had to be calibrated by carefully picking up the device and rotating it 360 degrees horizontally and vertically. A 60 x 60 cm plywood piece was used as a flight platform to avoid sand getting into the motors or cameras as the propellers start spinning. The device was manually ascended with a controller into about 15 m height after which autopilot was switched on and the UAV started conducting the automated mission according to the IPad-prepared flight path. Maximum flight time for the UAV was about 15 minutes restricted by the flight batteries and after each flight the used battery was replaced with a fully charged one.

Table 3. Basic info of the UAV datasets. * = mean T value from 2 measurements.

UAV data	Date	Reference temperature (°C)
AkasIta TIR+RGB	10.8.2016	14.7
AkasKuer TIR+RGB	10.8.2016	12.3*
Kuer 1 TIR+RGB	10.8.2016	12.3*
Kuer 2 TIR+RGB	7.8.2016	12.3*
Valkea TIR+RGB	7.8.2016	11.1
AkasValkea 1 TIR	10.8.2016	10.9
AkasValkea 2 TIR	10.8.2016	11.0
AkasValkea 3 TIR	10.8.2016	11.0
Akas TIR+RGB	9.8.2016	-
AkasValkea RGB	10.8.2016	11.0

4.2.2 UAV data processing

Pix4D software was used for the processing of the UAV TIR and ortho data similar to Faye et al. 2016. The program is intended for creating high-quality georeferenced maps and 3D-models from UAV imagery. Some pre-processing was required before the TIR images could be processed in Pix4D. Thermoviewer software was used for the processing and it included removing unneeded parts of the TIR flight such as the takeoff and descent of the UAV. There were also temperature scale jumps occurring between groups of consecutive images because of flat field correction (FFC) made by the thermal camera. When the FFC occurs at a high frequency, it generates heat that causes distortion. Temperature changes affect the camera and FFC enhances the image quality and reduces the temperature distortion, although because of lack of casing or protection for the camera during the flights some temperature shift still remained. To remove the temperature jumps, a drift compensation process in Thermoviewer was utilized: each flight was checked frame by frame and the FFC frames were marked after which the process produced a file without the scale jumps.

Ortho- and TIR imagery were imported with GPS data to Pix4D. Some images had inaccurate altitude information which needed to be corrected manually. After this the ortho images were ready to be processed, but the TIR images needed some more preparation before the processing. Images in the corners and turns of the flight paths needed to be disabled manually

as well as lines that crossed each other in an angle other than parallel or perpendicular were to be disabled.

There were four phases in the main Pix4D processing and some of them took hours at the longest. The phases included initial processing, a point cloud and mesh generation, a digital surface model, orthomosaic and index map generation, and index calculator processing. The first three phases were used on the ortho imagery and all four phases on the TIR imagery. After each processing phase a quality report was generated which showed different parameters that measured the success rate of the process. Sometimes some pre-processing steps had to be redone in order to get acceptable numbers for quality parameters. In the fourth phase (index calculator) absolute temperature values were acquired from the TIR radiance values by creating a temperature index with the equation 0.04*thermal_ir - 273.15 (Pix4D Support 2016). The finished mosaic TIR and index temperature maps were then exported as TIFF files. Mean pixel resolutions were 4.6 cm for the RGB imagery and 13.4 cm for the TIR imagery.

4.2.3 ArcMap GW discharge site classification and longitudinal temperature profiles

The thermal TIFF maps created with Pix4D were imported to ArcMap and GW discharge sites meeting the defined area and size requirements were identified by hand and divided into four different classes chosen or modified from classes used by Ebersole et al. 2003a, Korkka-Niemi et al. 2012 and Torgensen et al. 2012. The classes were selected or based on commonly used classes in literature taking into account the small-scale river environment of this study. The minimum requirement area of 0.50 m² for a GW discharge site used in this study is attained with 28 pixels in the TIR data with the average pixel resolution 13.4 cm. The high resolution ortho images were used as reference in the process to avoid identifying shaded terrestrial areas as GW discharge sites.

To examine the change in the stream ambient temperature along the rivers more precisely, longitudinal temperature profiles were created for each river section with UAV data. First, a centerline for the river was drawn in GIS by hand and points in 5 meter intervals were

constructed along the line. A 20–40 m area near the TIR mosaic image edges was not taken to account because the temperatures had an increasingly negative distortion closer to the edge. The temperature values at the point locations were then extracted from an index raster created with Pix4D using bilinear interpolation that calculates the point value as a weighted average of the nearest four pixels to it. Lastly, the extracted temperature tables were exported to Excel for temperature correction and for creating the profiles. A similar method for ambient river temperature extraction was used by Monk et al. 2013 where pixel values were picked from the center of the river and saved as the temperature samples.

In Excel the temperatures were adjusted according to the field reference temperature measurements (except for Akas TIR), because the TIFF values were displayed as too low due to the unprotected TIR camera resulting in a FFC correction too dense. Relative temperatures were however presumably displayed correctly, so only the absolute values were corrected 6–10.9 degrees upwards. Kuer 2 TIR had the smallest and AkasIta TIR the largest corrections. Finally, the discovered GW discharge sites were placed in the temperature profiles according to their positions along the rivers.

4.3 Landscape metrics analysis

4.3.1 GIS data and selection of the metrics

Relevant data for GIS analyses were downloaded from open data portals Paituli and Hakku and it included data from National Land Survey of Finland, Geological Survey of Finland and Finnish Environmental Institute. The data included a DEM, topographical maps, quaternary deposits, bedrock, land cover, river channels, catchment areas and GW areas (Table 4). The elevation accuracy of the DEM is on average 1.4 meters.

Table 4. Data used in the spatial analyses.

Data	Data source	Resolution	Year published
DEM	National Land Survey of Finland (NLS)	10 m	2015
Bedrock map	Geological Survey of Finland	1:100 000	2014
Quaternary deposits	Geological Survey of Finland	1:200 000	2012
CORINE land use	Finnish Environmental Institute (SYKE)	1:100 000	2012
Topographical base map	NLS	1:100 000	2015
Channel network	SYKE	1:10 000	2015
Watersheds	SYKE	1:50 000	2010
Groundwater areas	SYKE	1:20 000	2015

A 10 meter digital elevation model was used in the ArcMap GIS analyses. The DEM consisted of several pieces which were combined with the raster mosaic dataset function. The mosaicked DEM was analyzed and corrected for sinks or other flaws to create a depressionless DEM to avoid having discontinuities in the drainage network.

Four types of landscape features were used by Dugdale et al. 2015 for the correlation with the thermal refuges: drainage network, basin topography/geomorphology, watershed surface-/subsurface geology and basin land cover. These feature categories consisted of seventeen landscape metrics calculated with different methods from a 20 m DEM and corresponding optical imagery. Ebersole et al. 2003b metrics included wetted channel width-to-depth ratio, channel slope (=gradient) and sinuosity. Monk et al. 2013 used somewhat different landscape variables in their river refuge study compared to Dugdale's study: catchment area, stream length, catchment forest type and land use, soil types and bedrock geology, total precipitation/mean air temperature of the month of measurement, minimum/maximum/mean catchment slope/elevation and distance from mouth of river. The metrics used by Monk et al. 2013 were not used as an example for this study because of the lack of specific enough soil type data and with the interest mainly in local geomorphologic metrics.

For this study, four landscape metrics were chosen for the analysis based on the metrics used by Ebersole et al. 2003b and Dugdale et al. 2015: 1) channel sinuosity and 2) gradient, 3)

terrain slope and 4) entrenchment ratio. Availability of spatial data with an adequate scale was the most significant factor affecting the selection of the metrics. The scale of the study area is so small that a common 1:200 000 scale map provides too vague information for this kind of a specific analysis.

4.3.2 Metrics calculation with spatial analysis

The study area rivers were divided into 100 meter intervals in ArcMap and the metrics were examined in these 100 m sections except for entrenchment ratio where 500 m intervals were used. The 2012–2013 GW discharge site materials were then imported as point data for landscape metrics spatial analysis along with ortho imagery and the GIS data. The point data was connected to the 100 meter long sections so that each section has an identifier to be used with the calculated metrics. Each section was given a binary (occurrence/absence) and a count value of the discharge sites located in the section. This resulted in two different spatial datasets with the same metric values to be used in the statistical analyses: GW discharge site occurrence and count.

Stream sinuosity was calculated as an index with a downloadable tool for ArcMap where the result value represents the deviation of the river centerline from a straight-line distance. A straight section of a river will have an index value of 1 and a tightly meandering section will have a value closer to zero. The river thalweg is often used in sinuosity calculations, but with no adequate depth data available a river centerline was used instead (e.g. Elliott 2011). Rosgen 1994 on the other hand described sinuosity as the ratio of stream length to valley length but as a ready tool for ArcMap was available for the calculation there was no need for the stream-valley length comparison method.

River gradient values were acquired from the DEM along the channels as difference in height per 100 meters. Terrain slope perpendicular to the river was examined in the 100m river parts within a 100 meter buffer from both sides of the river. A slope raster was calculated from the DEM and mean slope values in degrees in the river sections were acquired by using ArcMap's zonal statistics tool.

Entrenchment ratio (ER) is defined as the stream flood-prone area width divided by bankfull surface width of the channel (Figure 9, Rosgen 1994, Kline et al. 2004). The ER was calculated in 500-meter intervals as opposed to the 100-meter intervals used with the other metrics. The bankfull width was measured by hand from ortho imagery at three places along a 500-meter section to obtain a mean bankfull value for the section. A downloadable ArcMap tool was used for measuring the flood-prone or valley width of a section. The tool required a valley centerline, polygon representation of the valley and points along which to calculate the widths. As there was no readily available data on the shapes of river valleys, the valley edges were defined by hand based on the DEM, terrain slope and ortho imagery (e.g. Elliott 2011, Torgensen et al. 2012). Vegetation patterns were also used as reference when estimating the extent of the floodplain as according to Stanford and Ward 1993 paleochannels in a floodplain are indicated by changes in riparian vegetation. Each river Äkäs, Kuer and Valkea were given an estimation of depth or relevant valley height (Äkäs 5m, Kuer 2–3m, Valkea 1–2m) and the valley edges were drawn according to the different layers. Five valley width measurements were used for each 500 meter section mean width calculation.

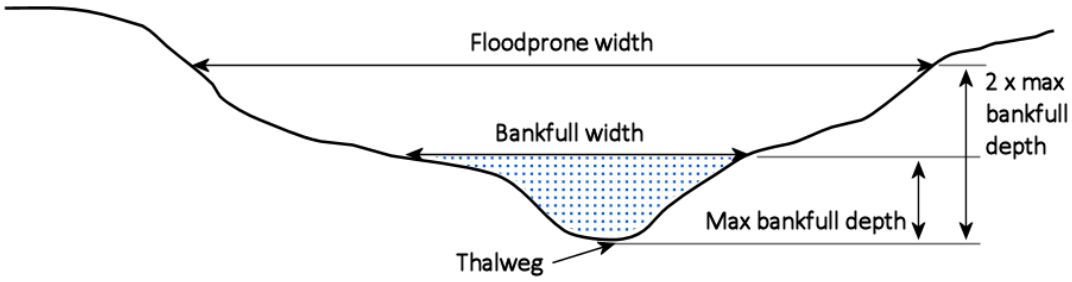

Figure 9. Principles for determining the floodprone and bankfull widths of a river for entrenchment ratio calculation (Modified after Kline et al. 2004).

Entrenchment and confinement were addressed as separate features by Rosgen 1994 whereas in Dugdale et al. 2015 study they were both used as descriptors of the channel-valley relationship. This study uses the terms similarly to Dugdale's study, entrenchment ratio as the measurable metric and later on valley/channel confinement as a describing term for the entrenchment.

4.3.3 Statistical analyses of the metrics and the 2012–2013 GW discharge site data

Statistical analyses of the data were performed with IBM SPSS 25 statistical software and Excel. The landscape metrics data was estimated for normality and data transformations were applied, as normally distributed data is used for linear regression (Ranta et al. 2012). In the discharge site and metric correlations, the site count and occurrence act as response variables and the metrics measurements act as predictor variables similar to Ebersole et al. 2003b. The aim is to find out whether the predictor values result in any changes in the response variables and possibly to discover connections between the predictor variables. A General linear model in SPSS was used for examining correlations between the discharge sites and the metrics with univariate tests. The model utilizes several different statistical models including linear regression. Various regression methods were used in landscape metrics analyses by Monk et al. 2013 and Dugdale et al. 2013, 2015. Associations within the landscape metrics were examined with Spearman's rank order correlation method.

5. RESULTS

5.1 UAV data

5.1.1 TIR and ortho imagery generated from Pix4D

Final pixel resolution of the UAV dataset varied a few centimeters between different sets, and the mean values were 4.6 cm for the RGB imagery and 13.4 cm for the TIR imagery (Table 5). A total area of 1.04 km^2 was covered with the RGB imagery and 0.63 km^2 with the TIR imagery. Examples of the TIR mosaic images with discovered GW discharge sites are in Figure 10 with Kuer 2 dataset and Figure 11 with Valkea and AkasValkea 1 and 3 sets.

Table 5. Acquired image resolutions and areas covered in the UAV imaging.

UAV data	RGB resolution (cm)	TIR resolution (cm)	RGB area (km^2)	TIR area covered (km^2)
AkasIta TIR+RGB	4.4	13.2	0.15	0.08
AkasKuer TIR+RGB	4.4	13.9	0.12	0.08
Kuer1 TIR+RGB	5.2	15.7	0.18	0.12
Kuer2 TIR+RGB	5.0	15.4	0.13	0.07
Valkea TIR+RGB	4.3	12.6	0.19	0.12
AkasValkea1 TIR		12.4		0.05
AkasValkea2 TIR		11.1		0.03
AkasValkea3 TIR		12.9		0.04
Akas TIR+RGB	4.6	13.1	0.09	0.04
AkasValkea RGB	4.3		0.19	
Area sum (km^2)			1.04	0.63
Mean resolution (cm)	4.6	13.4		

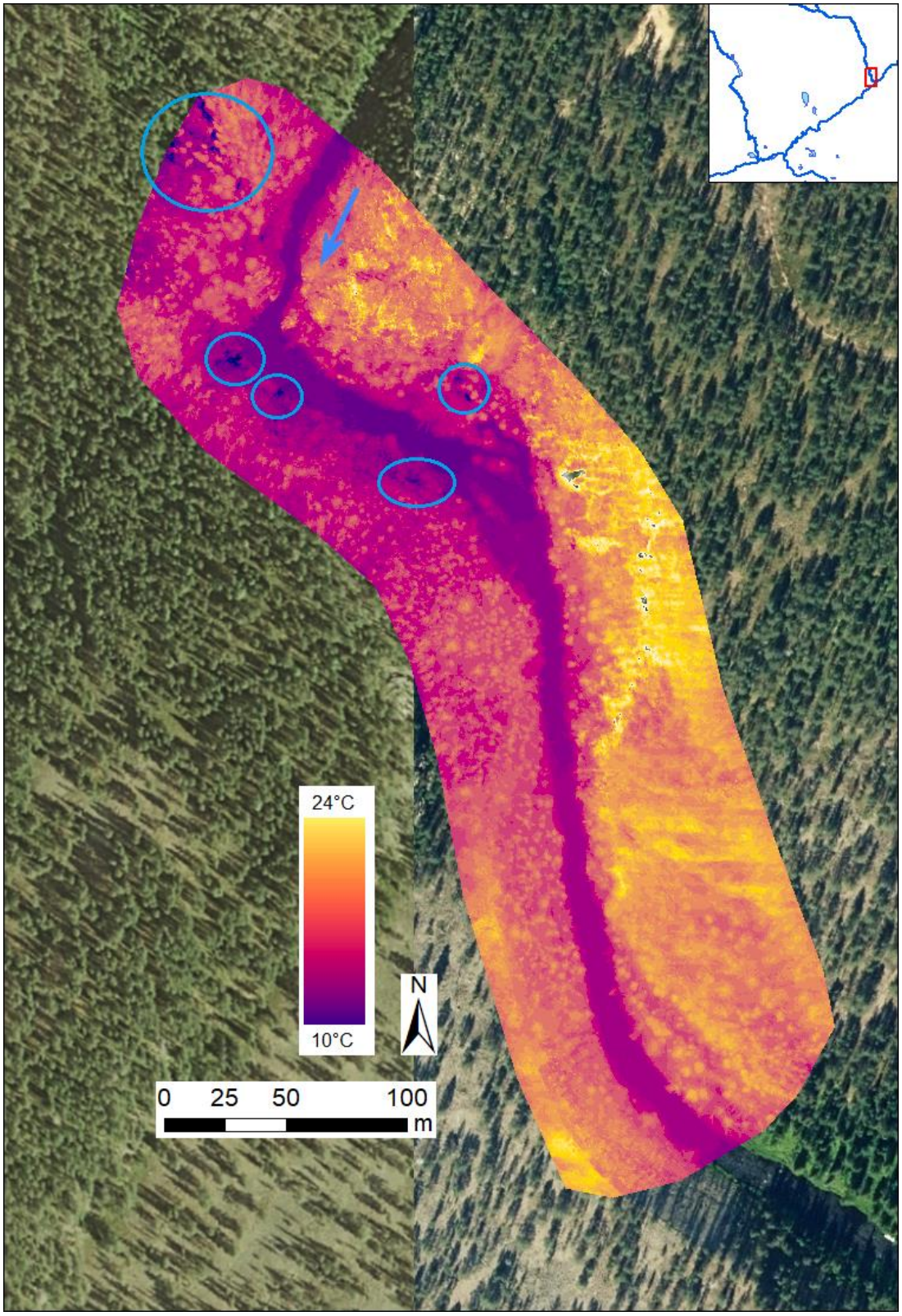

Figure 10. River Kuerjoki (Kuer 2) UAV TIR image dataset with discovered GW discharge sites marked with blue circles. Parts in the TIR mosaic with overexposure of light are shown as 'holes' in the image. Background ortho imagery from National Land survey of Finland (2010).

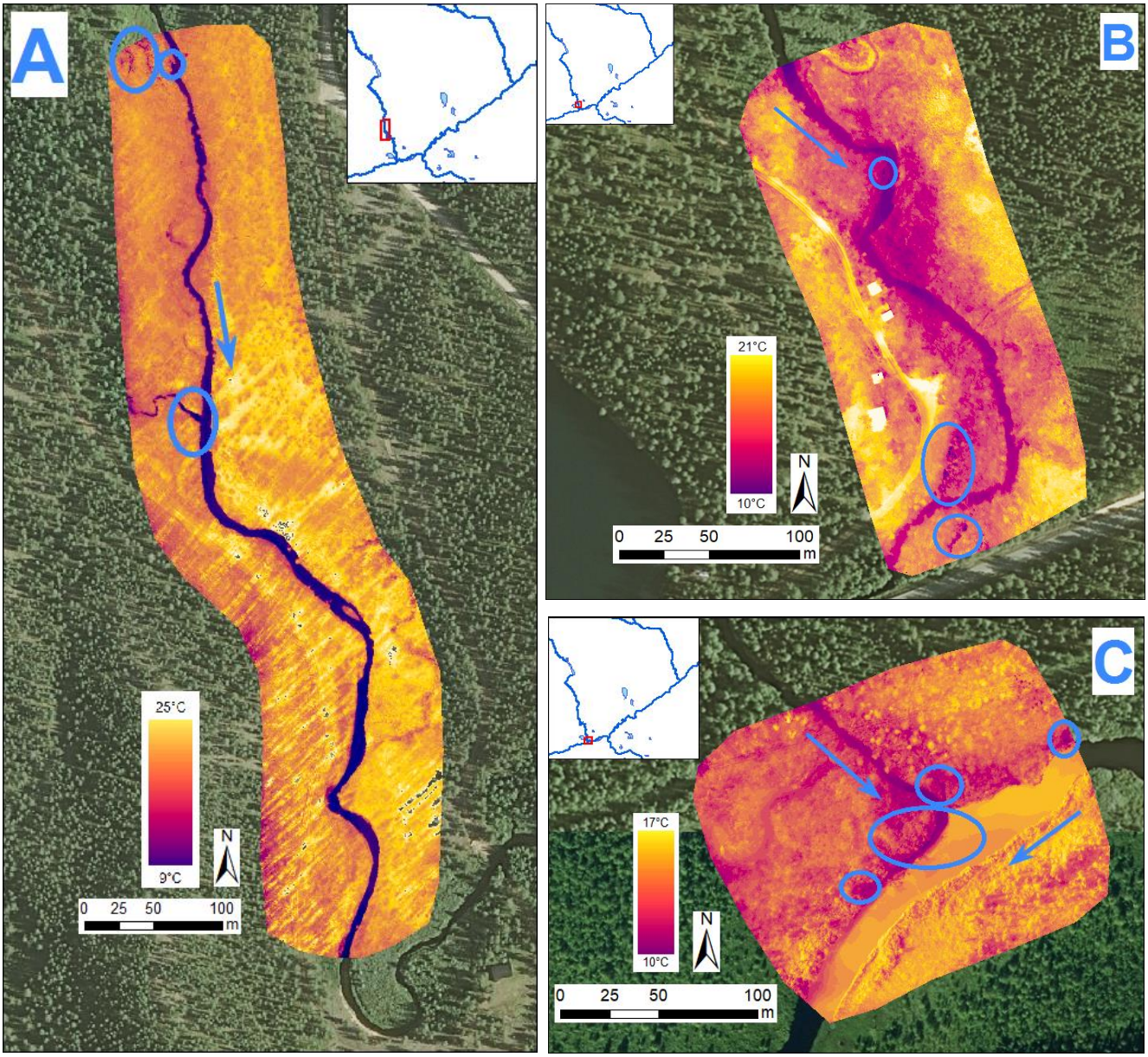

Figure 11. River Valkeajoki (A: Valkea, B: AkasValkea 1) and confluence plume of Valkeajoki to Äkäsjoki (C: AkasValkea 3) UAV datasets with discorvered GW discharge sites marked with blue circles. Parts in the TIR mosaic with overexposure of light are shown as 'holes' in the image. Background ortho imagery from National Land survey of Finland (2010).

5.1.2 GW discharge site classifications

The GW discharge sites were divided into four different classes: spring, diffuse seepage, relict channel and tributary confluence plume (Figure 12). A spring occurs as closely grouped cold spots in the river or the river bank. Diffuse seepage appears as a larger heterogeneous

area of cold spots next to the riverbank. Relict channel has cold patches along a clear channel shape that also has a generally lower temperature than the surrounding area. A tributary confluence plume occurs when a cold side channel discharges into the main channel, mixing gradually with the warmer water.

Similar classes used in the literature include cold alcoves, springbrooks (Ebersole et al. 2003a, Torgensen et al. 2012), tributary confluence plumes (Torgensen et al. 2012), ditches or creeks, springs and diffuse seepage areas near the riverbed (Korkka-Niemi et al. 2012). Cold alcoves are described by Ozaki 1988 as pools where "cold effluent groundwater, tributary flow, bank seepage or intragravel flow enters and is concentrated in the channel". Cold alcoves, springbrooks and ditches/creeks can be associated with the spring and relict channel discharge site categories used in this study. The relict channel class was modified from the existing categories to be used in this study.

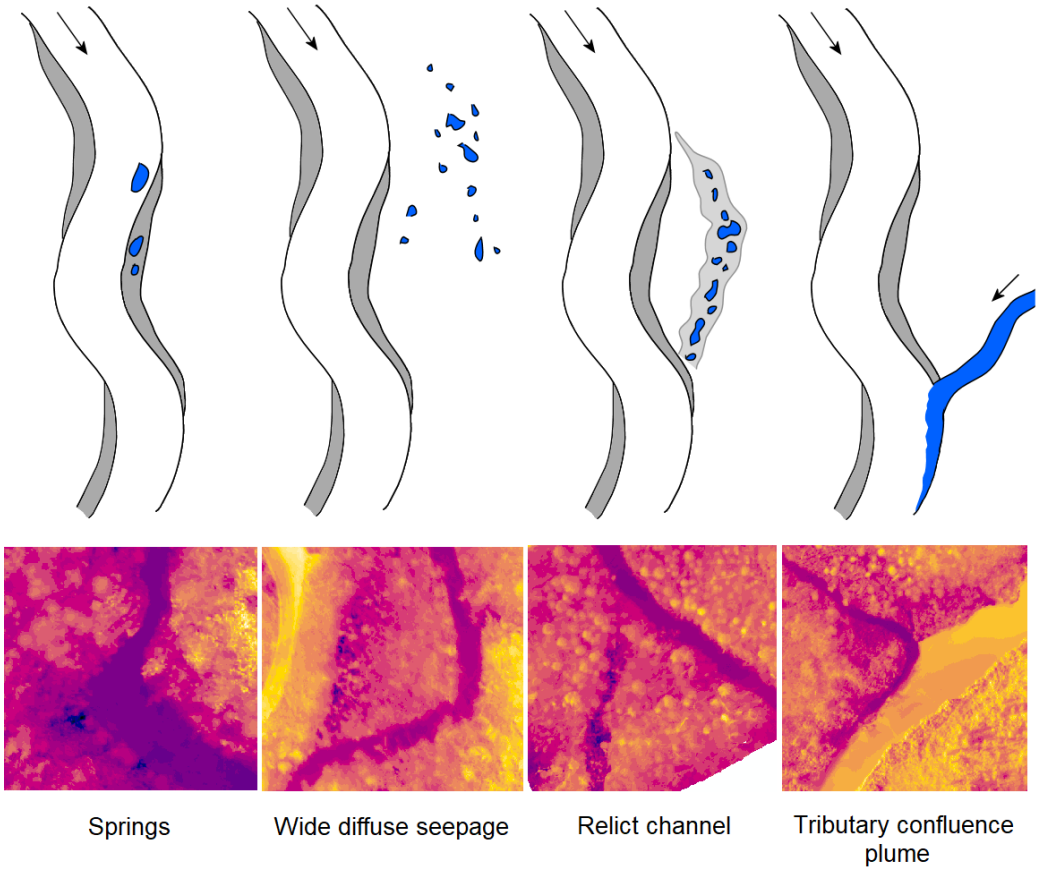

Figure 12. Selected GW discharge site types identified from the UAV data and TIR imagery examples.

Some of the UAV flights were overlapping one another so that the discharge sites were counted from a combined set (Kuer 1 and 2, AkasValkea 1, 2 and 3). No sites were found from AkasIta and Akas datasets. A total of 23 discharge sites were recognized from the data (Table 6), the most abundantly from AkasValkea with 10 sites (43 % of all found sites). Kuer had seven and Valkea and AkasKuer three sites. Spring was the most common type of discharge site with ten instances (43 % of all sites). Diffuse seepage had seven (30 % of all sites) and relict channel and tributary confluence plume three instances. Divided between the rivers, Valkeajoki had ten, Kuerjoki seven and Äkäsjoki six GW discharge sites.

Table 6. Groundwater discharge site types recognized from the UAV data.

UAV Dataset	Spring	Diffuse seepage	Relict channel	Tributary confluence plume	GW discharge site sum	Sum %
AkasKuer	1	-	1	1	3	13
Kuer 1,2	5	1	1	-	7	30
Valkea	1	1	-	1	3	13
AkasValkea 1,2,3	3	5	1	1	10	43
AkasIta	-	-	-	-	-	-
Akas	-	-	-	-	-	-
GW discharge site sum	10	7	3	3	**23**	
Sum %	43	30	13	13		100

5.1.3 Temperature profiles

Longitudinal temperature profiles were created from the UAV data from each river separately (Figures 14–23), and some of the UAV data was divided into multiple parts (Table 7). The study area locations of the profiles are presented in Figure 13. Discovered GW discharge sites were also placed in the profiles. Absolute water temperatures of the river datasets varied between 9.5 and 16.1 degrees and relative temperature changes between 0.79 to 2.89 degrees. The measured river length of the profiles varied between 80 and 680 meters. Valkea dataset had the coldest water and the greatest relative change in temperature. The warmest water was in the AkasIta dataset and the smallest change in temperature in Akas, which was represented by only a relative temperature. Comparing the rivers, Valkeajoki had the highest density of GW discharge sites with 7.5 per km, Kuerjoki had 5,7 per km and Äkäsjoki 4,9 per km.

Table 7. River water temperature scales of the UAV datasets.

Dataset	Figure 13 symbol	Profile name	Number of GW discharge sites	Absolute temperature range (°C)	Temperature change range (°C)
AkasKuer	D	AkasKuer - Äkäsjoki	3	13.2 – 14.7	1.46
	C	AkasKuer - Kuerjoki	-	11.6 – 12.8	1.17
Kuer 1,2	B	Kuer 1	2	11.0 – 13.6	2.67
	A	Kuer 2	5	11.4 – 13.0	1.60
Valkea	F	Valkea	3	**9.5** – 12.4	**2.89**
AkasValkea	G	AkasValkea 1	3	10.3 – 11.7	1.40
1,2,3	H	AkasValkea 2	3	10.5 – 11.6	1.10
	J	AkasValkea 3 - Äkäsjoki	3	13.1 – 14.1	1.03
	I	AkasValkea 3 - Valkeajoki	1	10.5 – 11.5	1.02
AkasIta	E	AkasIta	-	13.8 – **16.1**	2.30
Akas	K	Akas	-	-	**0.79**

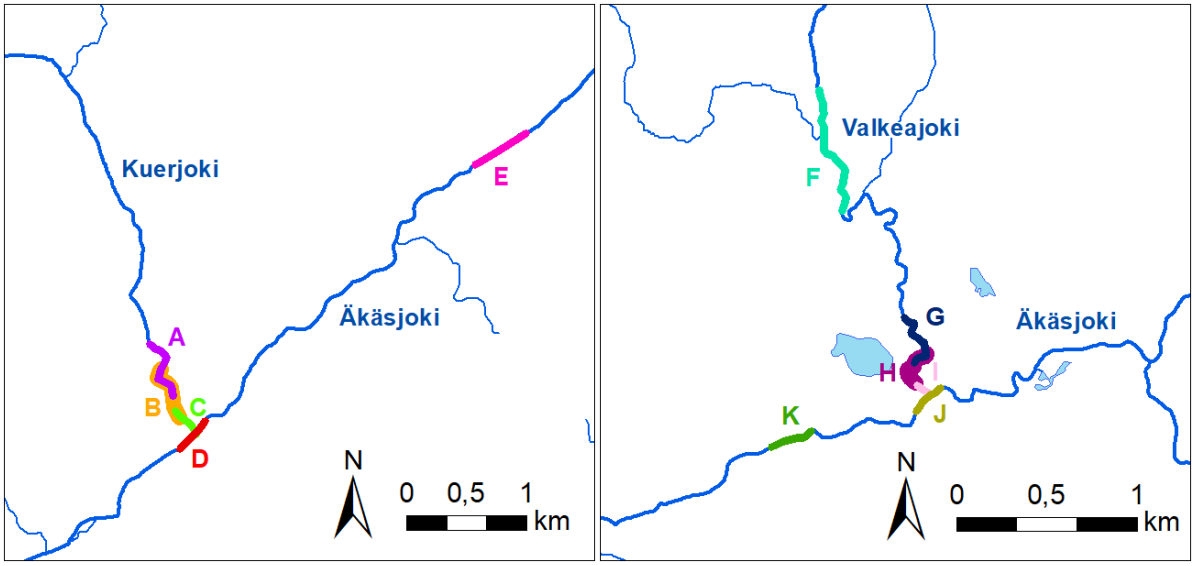

Figure 13. Locations of the longitudinal temperature profiles. A = Kuer 2, B = Kuer 1, C = AkasKuer - Kuerjoki, D = AkasKuer - Äkäsjoki, E = AkasIta, F = Valkea, G = AkasValkea 1, H = AkasValkea 2, I = AkasValkea 3 - Valkeajoki, J = AkasValkea 3 - Äkäsjoki, K = Akas (river network database, ©SYKE 2015).

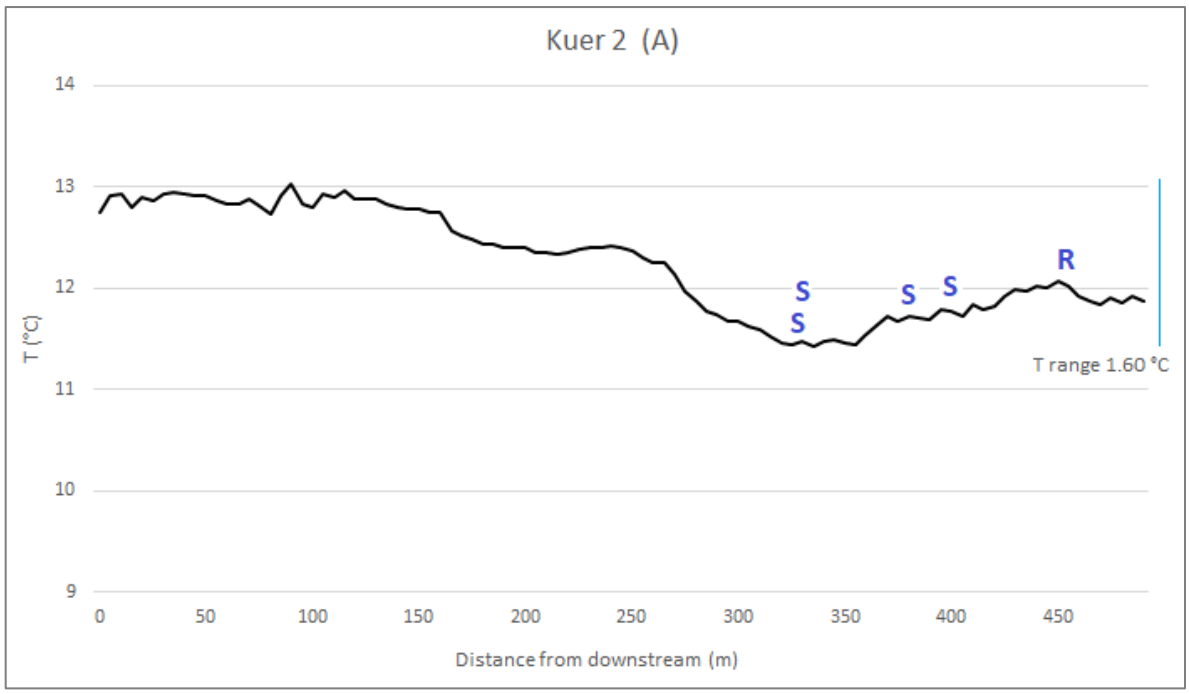

Figure 14. Absolute temperature of Kuerjoki river water as Kuer 2 UAV dataset (Letter A in Figure 13). Discovered GW discharge sites marked with S = spring, R = relict channel. Direction of river flow is from right to left.

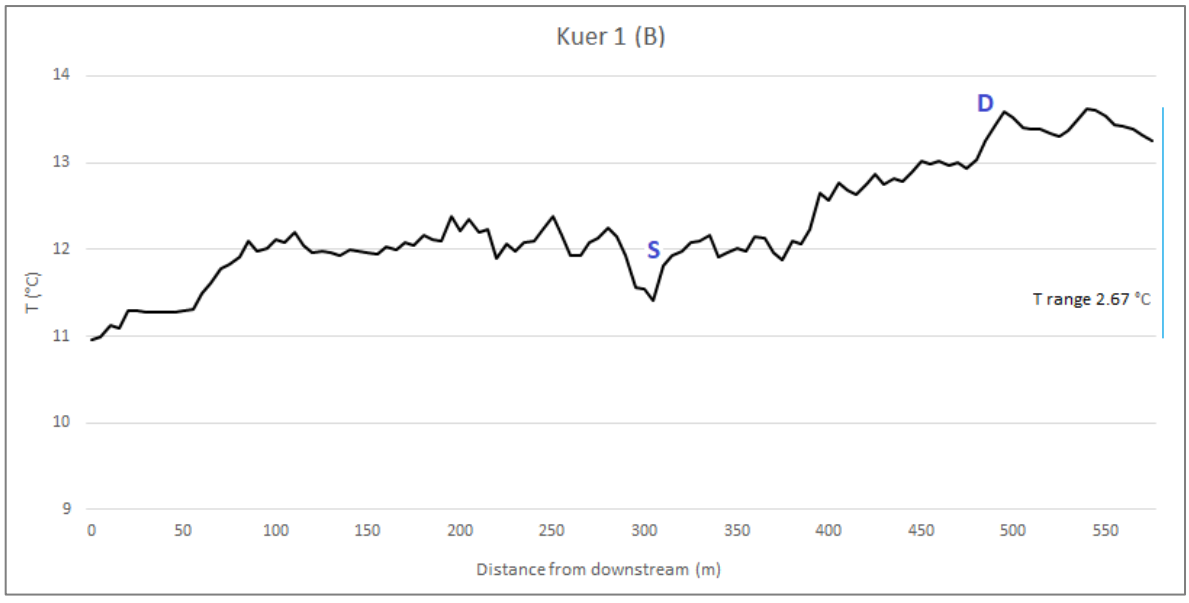

Figure 15. Absolute temperature of Kuerjoki river water as Kuer 1 UAV dataset (Letter B in Figure 13). Discovered GW discharge sites marked with S = spring, D = diffuse seepage. Direction of river flow is from right to left.

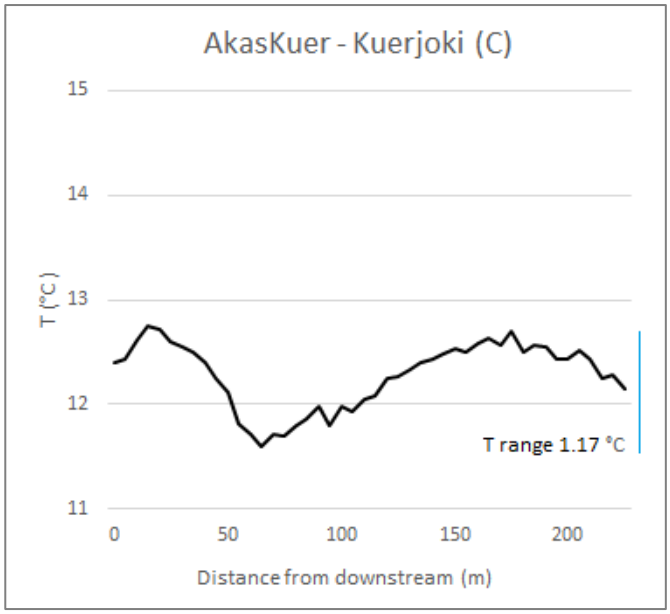

Figure 16. Absolute temperature of Kuerjoki river water as Akaskuer - Kuerjoki UAV dataset (Letter C in Figure 13). Direction of river flow is from right to left.

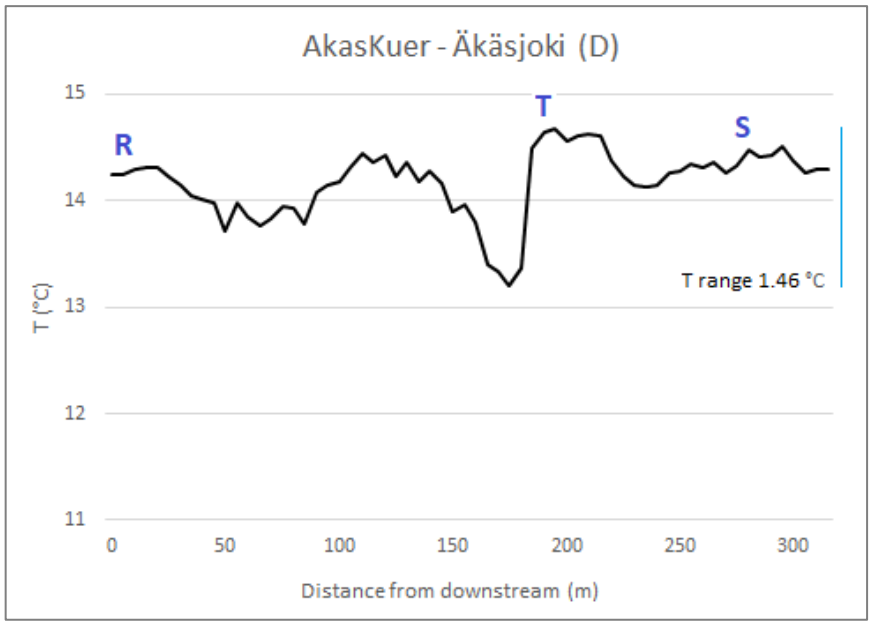

Figure 17. Absolute temperature of Äkäsjoki river water as AkasKuer - Äkäsjoki UAV dataset (Letter D in Figure 13). Discovered GW discharge sites marked with S = spring, T = tributary confluence plume, R = relict channel. Direction of river flow is from right to left.

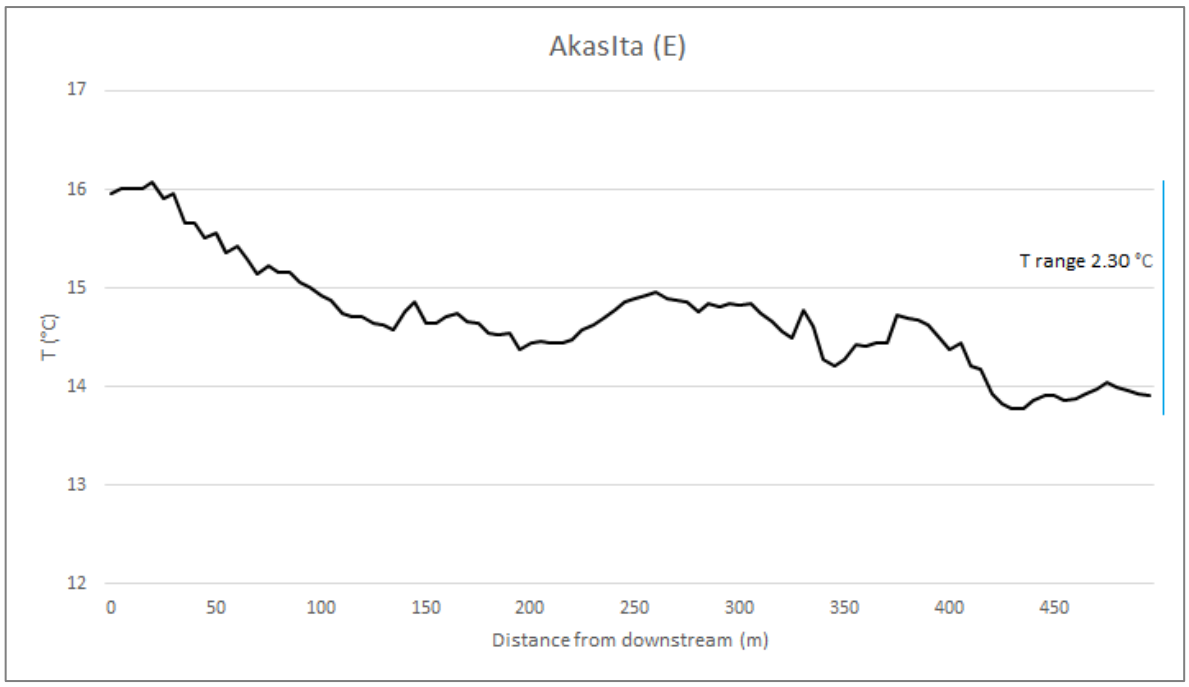

Figure 18. Absolute temperature of Äkäsjoki river water as AkasIta UAV dataset (Letter E in Figure 13). Direction of river flow is from right to left.

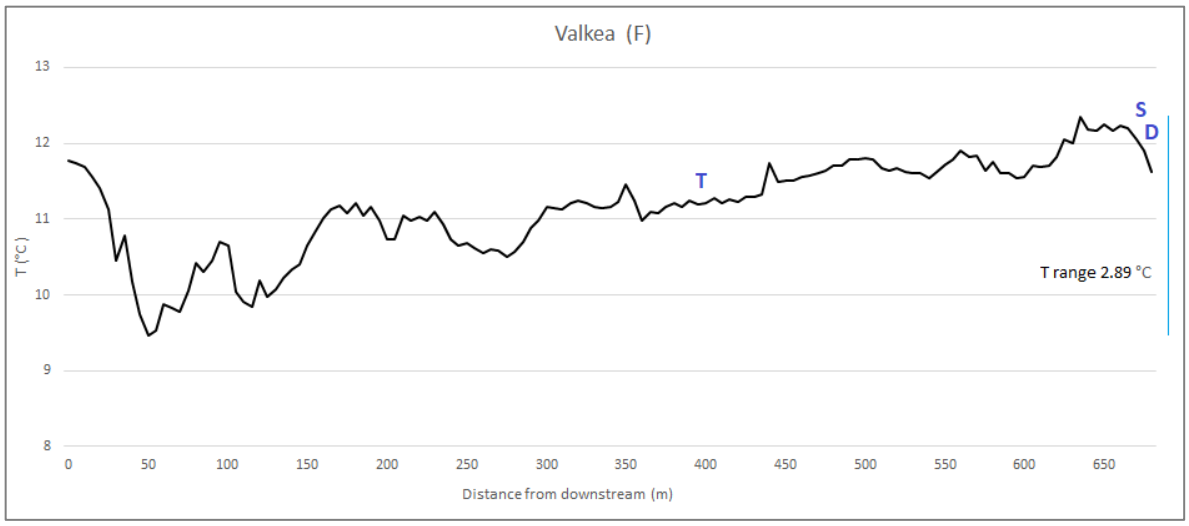

Figure 19. Absolute temperature of Valkeajoki river water as Valkea UAV dataset (Letter F in Figure 13). Discovered GW discharge sites marked with S = spring, T = tributary confluence plume, D = diffuse seepage. Direction of river flow is from right to left.

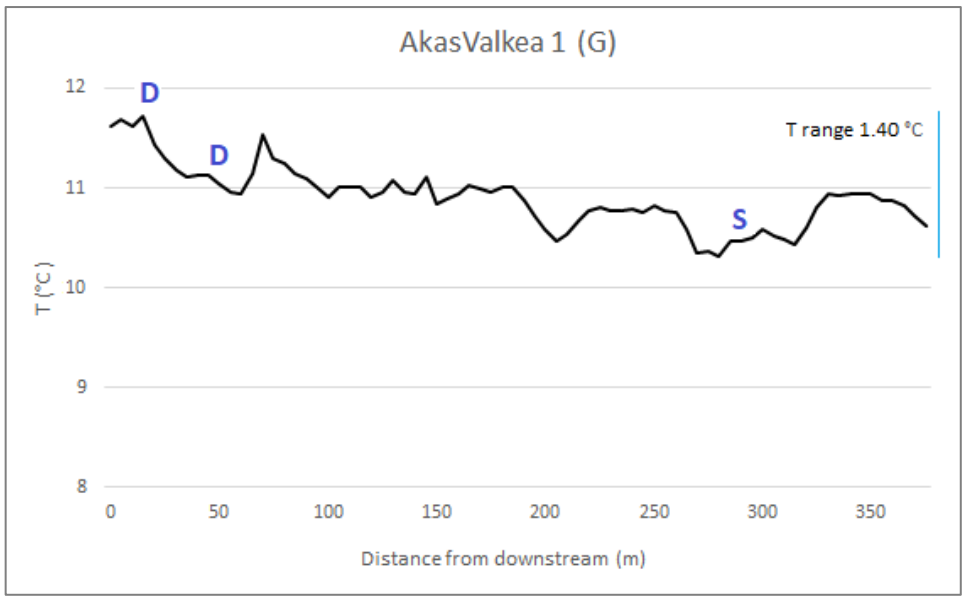

Figure 20. Absolute temperature of Valkeajoki river water as AkasValkea 1 UAV dataset (Letter G in Figure 13). Discovered GW discharge sites marked with S = spring, D = diffuse seepage. Direction of river flow is from right to left.

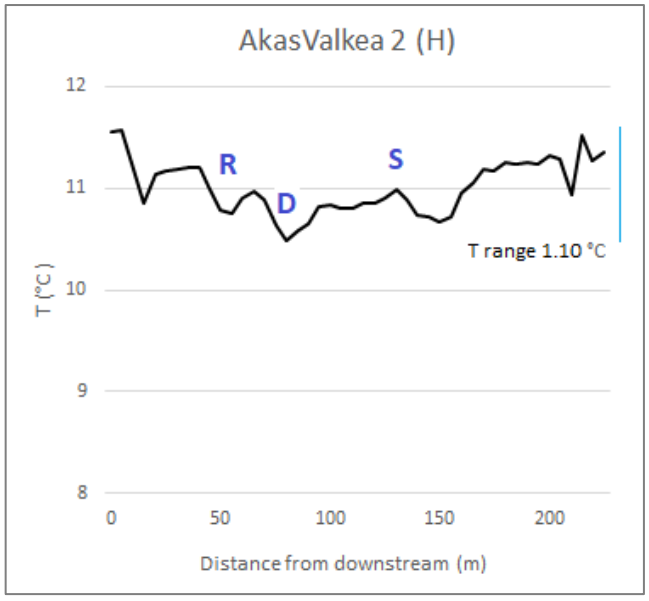

Figure 21. Absolute temperature of Valkeajoki river water as AkasValkea 2 UAV dataset (Letter H in Figure 13). Discovered GW discharge sites marked with S = spring, D = diffuse seepage, R = relict channel. Direction of river flow is from right to left.

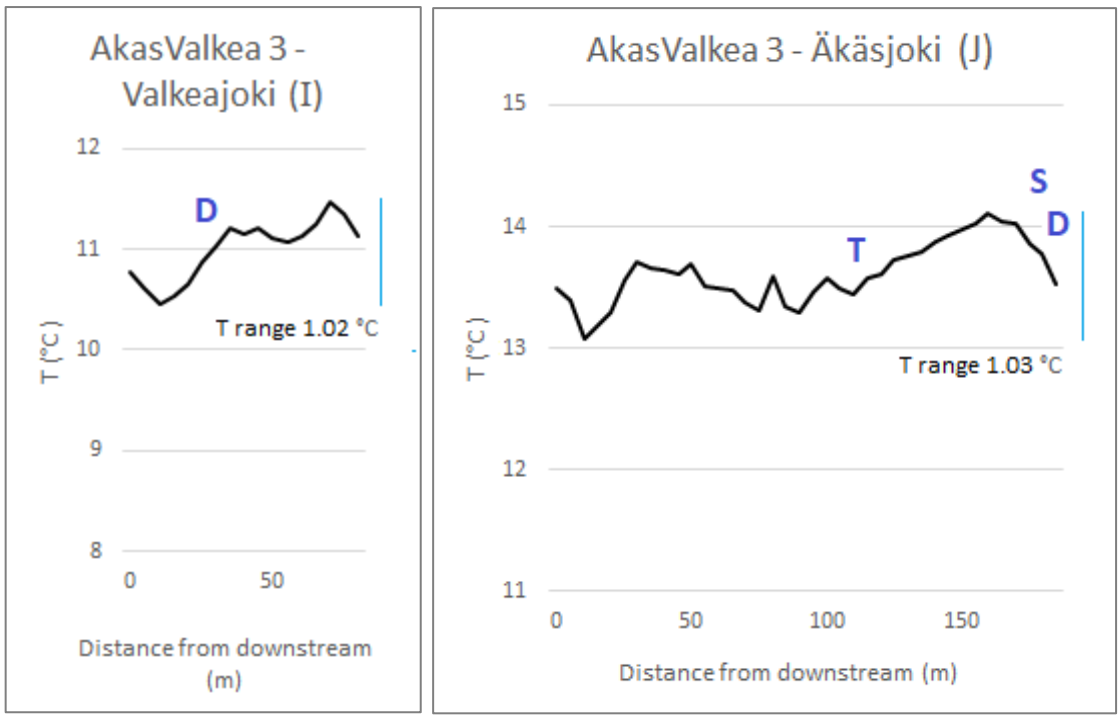

Figure 22. Absolute temperatures of Valkeajoki river water as AkasValkea 3 - Valkeajoki UAV dataset (Letter I in Figure 13) and Äkäsjoki river water as AkasValkea 3 - Äkäsjoki UAV dataset (Letter J in Figure 13). Discovered GW discharge sites marked with S = spring, T = tributary confluence plume, D = diffuse seepage. Direction of river flow is from right to left.

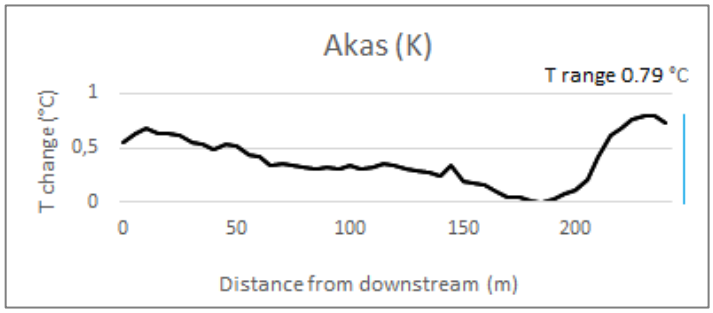

Figure 23. Relative temperature of Akasjoki river water as Akas UAV dataset (Letter K in Figure 13). Direction of river flow is from right to left.

General warming and cooling trends were both present in the profiles along with warm and cold anomalies. All rivers had relatively slow and abrupt changes, sometimes at the approximate occurrence of a GW discharge site but also without one. For example in Figure 17 profile (AkasKuer – Äkäsjoki) the temperature gets abruptly colder in downstream direction after the tributary point T where Kuerjoki discharges into Äkäsjoki. However in Figure 20 profile (AkasValkea 1) the temperature gets warmer to the downstream direction after two diffuse seepage areas near the left edge of the profile. In Figure 21 profile (AkasValkea 2) the relict channel and diffuse area seem to coincide with the lowest point of temperature and not before cooling or warming.

5.2 Landscape metrics

5.2.1 Descriptive statistics and data transformations

Descriptive statistics of the landscape metrics were calculated from the 2012–2013 TIR discharge site data with SPSS and Excel (Table 8). The skewness and kurtosis values, histograms and P-P -plots were used for examining the distribution of the metric values. Slope values were the closest to a normal distribution but still had a positive skewness. The other metrics were not normally distributed, gradient and entrenchment ratio with a positive skewness and sinuosity with a negative skewness. Sinuosity index values vary between 0.58 as most sinuous and 1 as most straight river section. Slope values vary between 0.47 as the flattest and 18.61 degrees as the steepest areas. Gradient values include also some minor negative values with a range from -0.25 to 5.89 meters of descent per 100 meters of river. Entrenchment ratio values range between 6.45 as the most confined and 97.86 as the broadest valley.

Table 8. Descriptive statistics and used transformation methods of the landscape metrics and mean metric values for the rivers.

	Sinuosity	Sinuosity arcsin	Slope	Slope $\log_{10}$	Gradient	Grad.+1 $\log_{10}$	Entrench-ment ratio	Entr. ratio $\log_{10}$
Range	0.42		18.14		6.14		91.40	
Minimum	0.58		0.47		-0.25		6.45	
Maximum	1.00		18.61		5.89		97.86	
Mean	0.94		4.82		0.33		23.37	
Std. deviation	0.07		2.70		0.61		23.45	
Skewness	-2.26	-0.97	1.71	-0.76	4.89	2.25	1.82	0.93
Kurtosis	6.19	0.77	4.87	1.83	32.84	7.2	2.15	-0.26
Mean (Äkäsjoki)	0.96		5.11		0.25		13.4	
Mean (Kuerjoki)	0.97		5.44		0.44		11.4	
Mean (Valkeajoki)	0.90		4.09		0.37		43.1	

Data transformations were applied on the metrics to approach normal distribution for linear regressions. The effects on skewness and kurtosis values are shown in Table 8, where a value closer to zero implies a more normal distribution (Ranta et al. 2012). A base 10 logarithm transformation was used for slope, gradient and entrenchment ratio similar to landscape or temperature variable transformations used by Ebersole et al. 2003b, Monk et al. 2013 and Dugdale et al. 2015. Gradient values were transformed as (gradient + 1) because of some negative values and zeros in the data, as values need to be positive for this transformation type. Sinuosity was transformed using the arcsine method, also used with some of the landscape metrics by Ebersole et al. 2003b, and it resulted in significantly better normalization than with the logarithm transformation.

The differences between mean metric values between the three rivers are also presented in Table 8. Further into the study the values are not separated between rivers in the statistical analyses. Kuerjoki has the most extreme values as it has the highest sinuosity index, gradient and slope and the lowest entrenchment ratio. Valkeajoki has two of the lowest values from sinuosity index and slope and the highest value from entrenchment ratio. Äkäsjoki has only one extreme value which is the lowest gradient.

5.2.2 GW discharge site and landscape metrics correlation

Correlations between the GW discharge site occurrence (binary) and count datasets with the landscape metrics were made with the General linear model in SPSS. In both binary and count datasets, gradient and entrenchment ratio gave a statistically significant correlation result ($p<0.05$) with the discharge site data (Table 9). The discharge site sets did not correlate significantly with sinuosity or slope ($p>0.05$). R^2 values measuring the strength of the correlation were 0.051 for the binary set and 0.082 for the count set.

Table 9. Linear regression correlation p-values for transformed landscape metrics and GW discharge site occurrence/count

	Site occurrence	Site count
Sinuosity	0.719	0.551
Slope	0.713	0.146
Gradient	**0.048**	**0.038**
Entr. ratio	**0.001**	**0.000**
	R^2 0.051	R^2 0.082

5.2.3 Correlation between the landscape metrics

Correlations between the different metrics were calculated using Spearman's rank order correlation analysis in SPSS. Spearman's correlation doesn't assume the data to be normally distributed but requires the data to be ranked before the analysis. There is statistically significant correlation ($p<0.05$) between all metrics except between gradient and sinuosity. The correlation coefficients are presented in Table 10. Entrenchment ratio shows negative correlations with the other metrics: moderate correlation with sinuosity and slope (correlation coefficients -0.41 and -0.47) and weak correlation with gradient (-0.25). Weak positive correlation is shown with coefficients of 0.17 between slope and sinuosity and 0.25 between slope and gradient.

Table 10. Spearman's rank order correlation coefficients between the landscape metrics with the significant ones marked with bold letters.

	Sinuosity	Slope	Gradient	Entr. ratio
Sinuosity	1			
Slope	**0.166**	1		
Gradient	0.026	**0.253**	1	
Entr. ratio	**-0.407**	**-0.465**	**-0.251**	1

6. DISCUSSION

6.1 Groundwater discharge in the study area

6.1.1 UAV GW discharge site classifications

The GW discharge sites discovered form the UAV data were divided into four different classes: spring, diffuse seepage, relict channel and tributary confluence plume. Springs, diffuse seepage and tributary confluence plume were the simplest categories to recognize. Korkka-Niemi et al. 2012 used in addition to their GW discharge site classes a discrete and diffuse discharge categorization. Rautio et al. 2017 used quite similar classes: discrete (spring brooks, cold side channels, cold alcoves, lateral seeps and wall-base channels), cold creek/tributary and diffuse areas. In a discrete discharge area the GW discharge appears as point-like and in a diffuse as a wider area consisting of multiple seep sources. The spring and tributary plume classes used in this study represent discrete discharge but the relict channel category has traits from both discharge types. The relict channel stretches to a wider area but at the same time the discharge is concentrated on the channel-like area or at the downstream end of the channel.

Cold alcove definitions resemble in many ways springs as a discharge point at the stream channel but e.g. Ebersole et al. 2003a states that an alcove can form at the downstream end of a relict channel. According to Torgensen et al. 2012 cold alcoves occur at places where

bedform topography causes strong vertical hydraulic gradients. Springbrooks often appear in relict channels according to Stanford and Ward 1993, Ebersole et al. 2003a and Torgensen et al. 2012. A relict channel is not listed as a GW discharge site class but as a platform or environment for springbrooks to occur in. Stanford and Ward 1993 state that springbrooks can be ephemeral so that during low flow season the brooks may decline into pools or disappear altogether. According to Torgensen et al. 2012 springbrooks are most common in coarse sediment streams affiliated with the latest glaciation with high hydraulic transmissivity, which fits the study area conditions in Hannukainen. The imagery data for this study was collected in low-flow conditions and so possible springbrooks may have been diminished. Also as there was no certainty of a floodplain or wetland origin required for a springbrook, the relict channel category remained.

Stanford and Ward 1993 used the term ‘wall-base channels’ about springbrooks that emerge from the substrata at a contact with the terrace or canyon walls. However e.g. Torgensen et al. 2012 and Dugdale et al. 2013 classify wall-base channels separate from springbrooks. The springs in Kuerjoki (Figure 10) occur at a very steep valley wall sequence so that if the other GW discharge site categories mentioned were utilized the wall-base channel or cold alcove category could have been used instead.

Spring was the most common type of GW discharge site with 43 % of all sites. 30 % of the sites were in the diffuse seepage class and relict channel and tributary confluence plume classes were both represented by 13 % of the sites. In Ebersole et al. 2003a study cold alcoves were the most common type of cold water patch with 52 % of all patches (77 altogether), cold side channels the second most common with 22 % and springbrooks the least common with 9 % of patches. In Korkka-Niemi et al. 2012 study wide diffuse seepage was the most common GW discharge site class with 55 % of all the sites (352 altogether). Spring was the second most common with 19 % and ditch/creek had 18 % of the sites. In Rautio et al. 2017 study the majority of discharge sites were in the discrete anomaly category with 77 % (including springbrooks, cold side channels, cold alcoves, lateral seeps and wall-base channels), 13 % were in the diffuse category and 10 % in the cold creek/tributary category (520 altogether). In Dugdale et al. 2013 study springbrooks, cold side channels, cold alcoves

and wall-base channels were not common classes with only between 5–7 % per class of the 253 total sites. Tributaries were the second most common class and included 26 % of all cold water areas. Wawrzyniak et al. 2016 study had more cold side channels (19 % of 63 sites) than tributary plumes (5 %). Only similar types of discharge sites in the literature were taken into consideration in assessing the commonness of the discharge site classes.

The commonness of the GW discharge classes differs quite widely between authors. Common classes in one study can be the least common in another. The comparison is challenging as each author has used slightly different methods to acquire and process the data and different definitions for the classes and for a GW discharge site or thermal refuge. The location of the study site and factors such as the geological landscape, vegetation, land use or climate affect the GW movements in the area and thus the ways the GW discharge areas appear in the area. Additionally the sparse amount of sites available (23) from this study restricts further speculations about the commonness of specific classes.

Some of this study's GW discharge sites could serve as thermal refuges for salmon and sea trout migrating to their natural spawning grounds. Of the chosen categories, tributary confluence plume seems to be the only class that the fish could access naturally. Some springs that are in the river channel could also fit as refuges, but many of the springs are located on the river bank, not in the channel itself which makes them inaccessible for the fish. The relict channel and diffuse seepage classes, spawning on higher ground in the river valley are not at all accessible for fish so they couldn't be count as thermal refuges.

6.1.2 Temperature profile analysis

The temperature profiles were examined manually along with the thermal and ortho images, elevation contours and DEM (for valley confinement estimation). Each profile is analyzed from right to left, upstream to downstream, starting from the two independent Äkäsjoki profiles with no GW discharge sites and in the end of the chapter causes for the temperature fluxes are considered more through literature.

In the Akas profile (Figure 23) relative temperature decreases rapidly over 0.5 °C at a wider channel section occurring right after a meander. After this the channel reverts to the previous width and the temperature gradually returns towards the original higher T. AkasIta profile (Figure 18) starts from 14 °C and gradually rises to 16 °C. The river section is quite straight and the width of the channel remains quite constant. The river channel is in a relatively confined valley in the AkasIta area and in the Akas area the valley is much wider.

Kuer 2 profile (Figure 14) has five discharge sites of which the first one upstream is a relict channel and the rest four are springs. A general warming trend from 11.9 °C to 12.8 °C is visible in this profile. The discharge sites occur in a quite short distance (150 m) along the river. The first three sites occur at gradually decreasing temperature and the last two springs just before a T rise. The river makes a tight curve just as the valley also becomes confined and the springs occur. The relict channel occurs just before the tight curve. The coldest part of the temperature profile is right after this meander in the middle of the springs at a wider part of the channel. After this the channel narrows and straightens again and the temperature rises along with it.

Kuer 1 profile (Figure 15) has two discharge sites that both seem to coincide with temperature decrease. Almost the half of the profile at the downstream end overlaps with the Kuer 2 profile. Kuer 2 dataset imagery is better quality so the discharge sites present there are marked only in that dataset. Nevertheless similar temperature trends are visible in the overlapping parts of the profiles. An overall cooling trend from 13.3 °C to 11 °C is visible from the Kuer 1 profile. The river valley is wider at the upstream part and gradually the valley walls become steeper, first on the eastern side of the river and then on both sides so that the channel becomes very confined. The diffuse area is quite far from the channel inside of a 90° meander. A cool water section along with the spring occurs after this same meander. The peak temperature of 13.6 °C occurs twice before the marked diffuse area at very narrow channel parts where small rapids also occur. This is a bit strange because it would make more sense if the water became colder with the mixing of possible cold water seeps from the river bed. The temperature does however cool right after the rapids.

AkasKuer - Kuerjoki profile (Figure 16, no discharge sites) displays altogether a T change of about 1 °C first rising slowly from about 12 °C to 12.7 °C and then slowly decreasing to 11.6 °C. Then a faster warming occurs to a peak of 12.8 °C with a drop afterwards. The Kuerjoki channel at this part is quite straight, steep from the west side and gentle on the eastern side. The channel widens a few meters and then becomes very narrow nearing the confluence point with Äkäsjoki. The coldest profile temperature occurs after the wide part of the river and the highest T at the very narrowest part of the river.

AkasKuer - Äkäsjoki profile (Figure 17) has three discharge sites of which the tributary confluence plume of Kuerjoki into Äkäsjoki clearly and abruptly decreases the temperature for over 1 °C from about 14.7 °C to 13.2 °C. At the same time the river channel becomes more confined as the valley walls become steeper on both sides of the river. After the initial confluence effect the T rises quite fast back but as the profile only shows temperatures from the middle of the river the effect of the plume that continues on the side of the channel is not seen in the profile. The thermal image shows that the plume continues all the way to the end of the profile. The other discharge sites don't seem to have much of an impact on the T, the spring causes maybe a small drop but the relict channel is at the very end of the profile so the effects of it are not visible.

Valkea profile (Figure 19) is the coldest and longest (ca. 670 m) of the profiles and it has three discharge sites. The greatest temperature changes don't occur at discharge site locations but before a large meander outside of the image at the downstream end. A general cooling trend can be seen from the profile until the last 50 meters when there is a sudden over 2 °C rise. The diffuse area and spring don't seem to induce cooling in the profile but the tributary is located at a cooling part of the profile although a clear plume is not visible other than from the thermal image. The first half of the river is quite straight and the width of the channel stays the same. Downstream of the tributary confluence the western side of the valley wall becomes steeper, the channel width is more variable and larger and tighter meanders occur. The temperature profile shows also more variation on the second half. There is also an old channel on the eastern side of the main channel that is shown colder than the average terrain. The temperature difference isn't large enough for it to be included in the relict channel

discharge site category but the old channel can nevertheless act as a funnel for GW flow into the main channel. Coincidentally, the main channel temperature starts to drop significantly right after the old channel confluence point. The channel is also wider at the point. The second lowest profile temperature occurs at the following tight meander bend and the lowest at a straight section after a leaner meander. The last 50 meter sudden temperature rise is strange as there is no significant channel, valley or sinuosity changes visible. There is however a massive 180° meander downstream of this river section so maybe it mixes the GW flow and the temperatures in some way.

AkasValkea 1 of Valkeajoki profile (Figure 20) has a general rising temperature trend from 10.6 °C to 11.7 °C and three discharge sites of which two diffuse areas occur with a rising temperature. The spring seems to have a small T decreasing effect but at the same time the channel also becomes wider. The river part is quite sinuous and has some tight meanders, one over 90°. The river water seems to be generally <0.5 °C colder in between meanders and at the meander it is warmer. The terrain also is quite cold between the meanders which could reflect intragravel flow and the GW cooling the ground.

AkasValkea 2 of Valkeajoki profile (Figure 21) has three discharge sites and is terrainwise similar to AkasValkea 1, as there is some overlapping between the imagery. No clear rising or decreasing trend in the temperature is seen as the profile starts at 11.4 °C and ends at 11.6 °C. The spring occurs simultaneously with decreasing temperature but the effects of the diffuse area and relict channel are harder to comprehend. These discharge sites are far from the channel itself and it's hard to compromise at what specific point the effect might become visible in the profile if at all. In this profile colder water temperatures seem to prevail also at the meanders. Although these specific meanders happen to have some tall trees and a road bridge that might distort the temperatures with for example shading.

AkasValkea 3 – Valkeajoki profile (Figure 22 I) is less than 100 meters long but has one diffuse seepage area and it seems to have a decreasing impact on the temperature as it goes down from 11.2 °C to 10.5 °C quite rapidly. The diffuse area here is the whole area near the

confluence point of Valkeajoki and Äkäsjoki and cold water seeps widely to the end part of Valkeajoki. The area is very flat.

AkasValkea 3 - Äkäsjoki profile (Figure 22 J) has three discharge sites and shows a slight decreasing temperature trend after an initial T rise although the start and end T are both 13.5 °C. The discharge sites show no clear correlation with temperature decrease in the profile but on the other hand the spring and diffuse seepage at the upstream end of the river coincide with a T rise. The cold confluence plume of Valkeajoki is clearly visible in the thermal image but as the plume stays at the west side of the channel it doesn't show on the profile. A peak high temperature of 14 °C occurs after a meander at a narrow channel part after which a wider section of the channel and slightly colder water prevail until the channel narrows gradually again and the water warms back up too.

There are some recurring traits between the temperature changes, discharge site locations and the river morphological features examined here. All of the discovered springs and diffuse seepages were situated only at somewhat meandering sections of the rivers. At almost half of the profiles channel widening was associated with water temperature drop in the channel or at the end of a wider part of the channel. As common was the narrowing of the channel leading to warmer temperatures. Almost as common a trait was lower temperatures occurring after a meander or between meanders. At a larger scale a more confined valley seemed also to occur with lower temperatures. Also generally with a confined valley, higher sinuosity and alternating channel width the temperature profile became more variable.

In Torgensen et al. 1999 and Dugdale et al. 2013 studies warm temperature peaks in temperature profiles were caused by shallow, exposed reaches with relatively wide valleys where the sun effectively warms up the water and GW contribution to the channel decreases. Cold troughs were caused by a deeply confined and shaded canyon. According to Dugdale et al. 2013 valleys with steep walls are also likely to have more GW discharge because of increased hydraulic head due to a raised aquifer. In Torgensen et al. 2001 study rapid cooling or warming in the profile was caused by tributary inputs. Gradual temperature changes over a 5-10 km distance were associated with watershed scale geomorphic, riparian and

hydrologic processes such as the proximity of wetlands or the widening of the main channel. Dugdale et al. 2013 state that gradual warming was observed with a smaller channel gradient and a wider channel. These allow the water to warm up effectively because of the slower flow speed and increased surface area of the river. A generally colder river was characterized by a proximity of large wetlands and an abundance of springbrooks emerging from the wetlands increasing the GW input to the river.

6.1.3 Geomorphological features and land use effects on GW discharge

According to Torgensen et al. 2012 at a basin and subbasin scale thermal refuges are mostly driven by elevation, topography, geology, gradient and interactions between surface and subsurface hydrology. Influential factors include also vegetation, soils and land use. The stream bed sediment composition and the shape of the river bed also have an impact on the occurrence of the GW discharge sites (Rautio et al. 2015). A fine-grained stream bed can lead to lower number of discharge sites due to the lack of preferential flow paths for GW. Rapid zones in the river can cause a drop in measured water temperatures because of mixing of thermally stratified water layers. The riverbed is also coarser in the rapids so GW discharges easier into the stream. Meander bends and stream channel narrowing affect the temperatures through mixing the same way (Rautio et al. 2015). Meandering seemed to lower the temperatures in this study, but narrowing channel seemed to lead more often to higher temperatures.

Bounded alluvial valley segments channel cool subsurface flow back into the river channel (Torgensen et al. 2012 and Dugdale et al. 2015). In this kind of segment the river valley widens and becomes less confined and typically at the downstream end where the channel becomes again more confined, cold water discharges back to the river. In this study colder water temperatures often prevailed at wider sections of the river or at the downstream end of the widening. The scale is however smaller but perhaps similar subsurface flow conditions could apply at a place like this.

Sudden changes in gradient might contribute to the incidence of downwelling and upwelling zones and so to potential thermal refuge occurrence (Torgensen et al. 2012). At reach scale, alluvial valleys with high sinuosity, numerous subsurface flow paths and alluvial fans are more likely to have an increased thermal diversity. The sinuosity effect is explainable by river high curvature zones draining a larger watershed area than a straighter river section (Dugdale et al. 2015). The increased thermal diversity in more sinuous river segments can be seen in the UAV data inventory as more sinuous river segments were clearly more thermally diverse than straighter sections. Also the coarse-grained riverbeds could enable extensive subsurface flow patterns in the area.

According to Stanford and Ward 1993 at a valley segment scale, stream water downwells upstream and upwells back at a suitable location downstream. Semi-confined valleys act as these kind of locations, as they have usually a moderately extensive sub-surface flow network, permeable alluvial deposits and due to some sloping a sufficient water table hydraulic gradient for GW upwelling. In Wawrzyniak et al. 2016 study this kind of upwelling was presumed at a high side seep density location after a segment of canyon-like, confined narrow channel and a large meander. These kind of upwelling locations create suitable conditions for floodplain depressions and wetlands and thus for the formation of thermal refuges such as springbrooks, cold side channels and cold alcoves (Dugdale et al. 2015). This agrees well with the UAV findings of this study as colder water seemed to occur in wider parts of the river after or between meanders and narrower parts of the river had warmer water. On the other hand more confined sections of the river seemed to have colder water.

A general overview of the land use map at the vicinity of the 2012–2013 discharge sites doesn't seem to have a significant impact on the commonness of the sites. All of the discharge sites are located at the coniferous/mixed forest and woodland/shrub categories and no visible differences in the amounts of discharge sites can be observed between these areas. The quaternary deposits map seems to have some effects on the GW sites occurrences however. In Valkeajoki and Kuerjoki, areas where the river channel lays entirely in the coarse-grained deposits GW discharge sites occur the most often. Areas with bedrock outcrops or diamicton seem to have slightly less discharge sites. This seems reasonable as coarse-grained deposits

have higher permeability leading to increased GW flow and seepage. However in Äkäsjoki there are areas with coarse-grained deposits on one side and diamicton on the other side of the river with more GW sites than areas with solely coarse-grained deposits. A possible cause for the increased GW discharge could be the moderately confined and deep valley of that part of the river creating otherwise favorable conditions for GW upwelling.

Examining the land use or Quaternary deposits in accordance with the UAV discharge sites was not considered reasonable because of the small amount of refuges, small covered areas and inadequate scales of the maps.

6.1.4 Comparison of GW discharge in the UAV and 2012–2013 TIR results

The GW discharge site classes determined from the UAV data in this study differed partially from categories used in the 2012-2013 TIR data. Categories used in the data were discrete anomalies (including springbrooks, cold side channels, cold alcoves, lateral seeps and wall-base channels), cold creeks or tributaries discharging into a main channel and diffuse anomalies with a varying size (Rautio et al. 2017). There are generally less discovered GW discharge sites at same areas in this study than the 2012–2013 TIR data.

Valkeajoki had the highest density of GW discharge sites with 7.5 per km in the UAV data and also in the 2012–2013 GW site data with a mean of 15.1 sites per km (Table 2 in p. 18). Kuerjoki had the next highest density with 5,7 sites per km in the UAV data and 11.1 sites per km in the 2012–2013 data. Äkäsjoki had the lowest GW site densities in both datasets: 4,9 (UAV) and 5,7 (2012–2013).

In Dugdale's et al. 2013 study thermal refuges were counted at six different occasions over a timescale of three years and most of the refuges (60.6%) were only identified once during the surveys. Only one refuge was present in all six surveys. Wawrzyniak et al. 2016 had similar findings, as in their three-campaign study over four years the majority of the cold water patches (52%) were observed only once. This could explain partly the differences between the GW discharge site locations, amounts and densities of this study and the 2012–

2013 data. In three to four years between the data acquisitions of these datasets, the locations of the GW discharge sites could have changed significantly. Also an effecting factor could be the usage of different techniques for data accumulation and processing and definitions for the discharge sites. Overall the comparison of the two datasets is challenging because the UAV areas are so small that they only provide snapshots of the study area when the 2012–2013 data provides information from the whole area.

6.2 Connections between groundwater discharge and landscape metrics

6.2.1 Statistic correlations

The General linear model produced low R^2 values (0.051 for discharge site occurrence and 0.082 for count) for the significant metrics. The R^2 value measures how well a regression model fits the actual data, as in it is a measure of the overall accuracy of the model. A model with a high R^2 (closer to 1) predicts the values in the model well and with a low R^2 (closer to 0) poorly. The lower the R^2, the more variability is in the model values (e.g. Ebersole et al. 2003b). The low R^2 value means that gradient and entrenchment ratio have at least a small effect on the discharge site occurrence and slightly more significant effect on the discharge site count along the rivers, but a large part of the variance in the data is left unexplained.

Diagrams describing the correlation between GW discharge sites and the significant metrics of the General linear model (entrenchment and gradient) were made with Excel using the untransformed values (Figures 24 and 25). The metric values were binned into 15 equal size classes and sorted according to the metric value. Then a mean discharge site count and mean of the binary values was counted for each class. The entrenchment ratio (ER) graph (Figure 24) has larger differences between adjacent values than the gradient graph (Figure 25). In both graphs the discharge site count and binary averages follow approximately the same increasing and decreasing patterns. Both diagrams show an increase of discharge site values approximately at mid- and high-range metric values and lower site values at mid-high metric values. However, as the ER values had a very high standard deviation (23.45 in Table 8), further inspection of this diagram was not considered reasonable, as patterns in the diagram

are very likely chance variation in the data. The standard deviation of the gradient values was not too high (0.61 in Table 8) so Figure 25 could describe actual relationships of the data and the discharge sites.

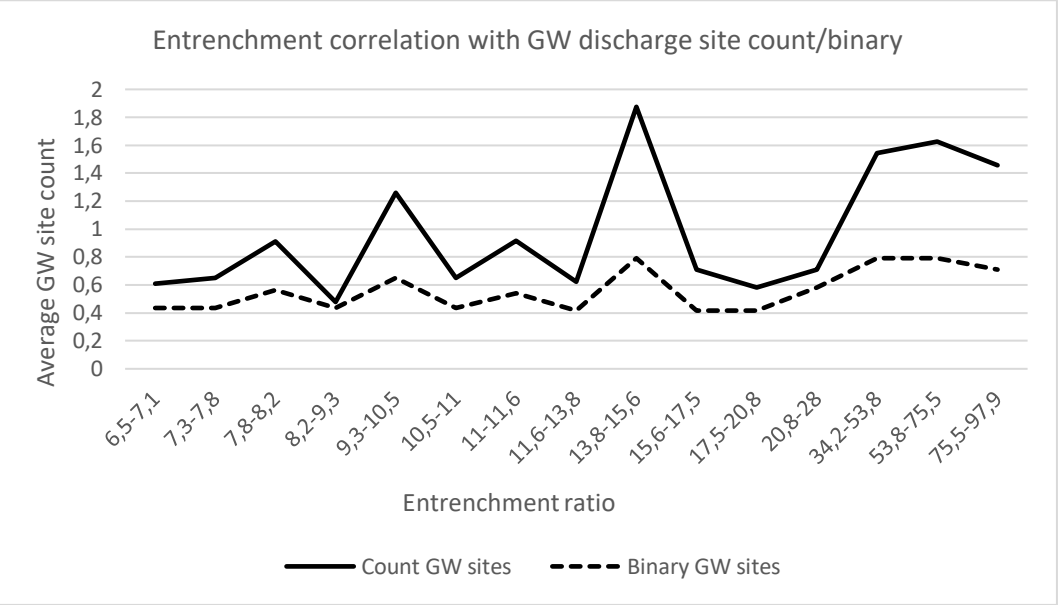

Figure 24. Entrenchment ratio correlation with average GW discharge site counts.

The gradient diagram (Figure 25) shows a relatively consistent relationship between the metric and discharge site values. The site values are the highest (count 1.2-1.4 and binary 0.6-0.7) with the lowest, mid-range and high gradient values. Mid-low and mid-high gradient values produce lower site values (0.4-0.8 and 0.2-0.6).

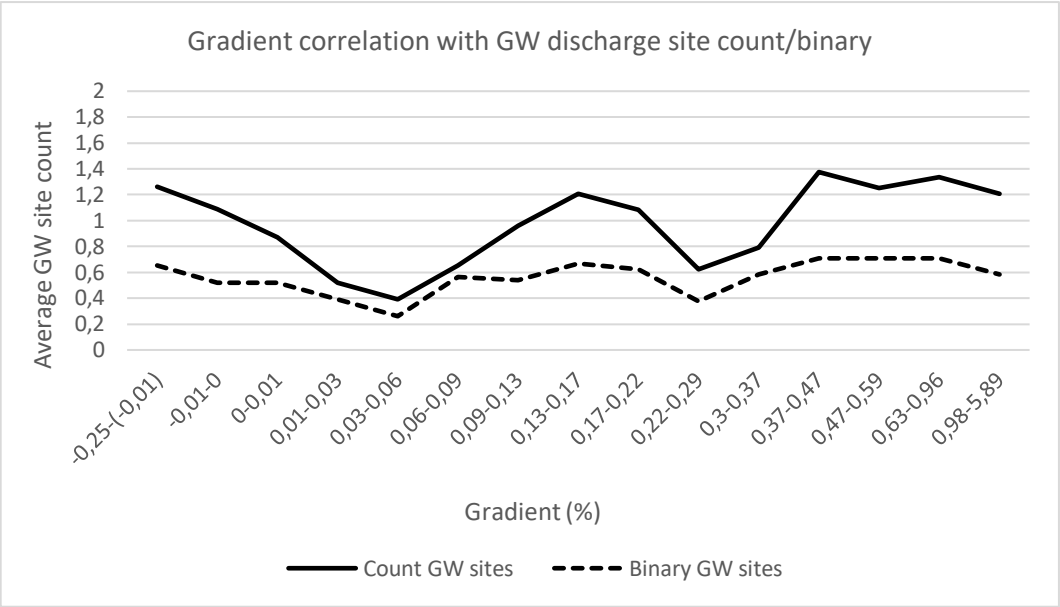

Figure 25. Gradient correlation with average thermal GW discharge site counts.

The General linear model p-value correlation coefficients don't describe the direction or intensity of the correlations between the significant discharge sites and metrics. For this, Pearson's correlation method was used: it gives a correlation coefficient and a significance value between two variables (untransformed significant metrics and discharge data, Table 11). ER correlated significantly with the discharge site datasets but gradient did not, so further analysis of the gradient diagram (Figure 25) was not continued. Gradient having a significant effect in the General linear model but not on the Pearson correlation could be due to the low R value attained from the GLM and the use of transformed variables.

Table 11. Pearson's correlation coefficients and p-values of the GLM significant metrics and the discharge data.

	Gradient	Entr. ratio
Site occurrence		
- correlation coefficient	0.034	**0.183**
- significance	0.522	**0.001**
Site count		
- correlation coefficient	0.053	**0.232**
- significance	0.320	**0.000**

According to the Pearson correlation coefficients, ER has a positive weak impact on the discharge site occurrence (0.183) and count (0.232). Thus, when ER values grow and the valley openness increases, the occurrences and amount of GW discharge sites increase in average, and as the valley gets more confined the discharge sites occur less often. As the correlation is weak, much of the effects on the discharge amounts come from elsewhere.

Gradient didn't correlate significantly with the cold water patches in Ebersole et al. 2003b study. In the study, mean channel width-to-depth ratio was the only statistically significantly correlating metric with the density of cold water patches, with a negative correlation (R^2=0.22). Quite similar to this study the low R^2 value leaves much of the model unexplained. Wetted channel width-to-depth ratio could be compared to entrenchment ratio, as both ratios are relatable to channel or valley confinement. Similar to ER, a smaller channel width-to-depth ratio would represent a more entrenched/confined channel. This would suggest that a confined channel in Ebersole's study has more cold water patches and a wide shallow channel less patches, which differs from results of this study where a confined valley has less discharge sites and a wide, open valley has more discharge sites. The comparability of these metrics is probably not this simple though so differences in the results are not surprising.

Dugdale et al. 2015 divided their thermal refuge dataset quite similar to this study into binary and density parts although this study used count instead of density in the correlation analyses. In Dugdale's study channel slope (gradient) didn't correlate significantly with the metrics but entrenchment ratio had a significant correlation with the discharge site density with moderate values producing the highest discharge site densities and extreme low or high values producing the lowest densities. The high ER value-low density is a complete opposite result compared to this study, although it could be possible that medium ER values have higher discharge site occurrences but the high standard deviation of the ER prevents examining closer the connections to the discharge data. Dugdale et al. 2015 state that moderate entrenchment values represent semi-confined valley segments that are associated with slope breaks that drive GW upwelling at the floodplain. This upwelling is absent in especially confined or unconfined valleys where the no slope breaks occur.

In Dugdale et al. 2015 study, channel curvature and tributary valley distance had a distinctive influence on the occurrence of individual thermal refuges, with higher curvature values occurring with higher numbers of refuges. Channel curvature and sinuosity were two separate metrics, with the curvature at a local, channel unit scale and sinuosity at larger scale. The lack of correlation between sinuosity and refuge occurrence is thought to be caused by a too vague scale. This study's similar lack of correlation between sinuosity and the discharge sites could be caused also by scale incompatibility. The used 100 meter intervals can include multiple meanders when only the immediate environment of the discharge site is relevant. In Ebersole et al. 2003b study sinuosity also did not correlate with the cold water patches.

6.2.2 Associations between landscape metrics

The Spearman's correlation (Table 10 on p.43) shows the direction and intensity of the correlation unlike results from the General linear model. There is statistically significant correlation between all metrics except between gradient and sinuosity. When entrenchment ratio gets smaller meaning the river valley gets narrower and more confined, the slope of the near-river terrain becomes steeper and vice versa. Also, with a more confined valley the channel gradient becomes steeper and the river flows faster. Sinuosity index grows when valley confinement increases, meaning that the river is less sinuous in a more confined valley. Positive correlation between slope and sinuosity index indicates that when the terrain slope increases the river is again less sinuous and vice versa. Positive correlation between slope and gradient shows that as the slope steepens the stream gradient also grows.

So to combine the discharge site occurrence and count data with these observations the most interesting values to examine are especially the high ER values which represent wide valley segments and have the higher discharge site counts according to the Pearson correlation. With the moderately confined option the other morphological features are also moderate with no extremities. Some sloping next to the channel, some lean meanders and not too fast flowing waters. With the wide valley there are gentler slopes, a more sinuous channel and smaller gradient with slower flow.

The lowest discharge site counts for ER according to the Pearson correlation are at low values representing the most confined open valleys. So according to the Spearman analysis between the landscape variables, with a confined valley the slopes are steeper, the channel is straighter and steeper with faster flow.

6.2.3 Differences between the rivers

The mean landscape metrics for each studied river differed to some extent from one another (Table 8 on p.41). According to the metric values, Kuerjoki flows the most straightly and steeply, has the steepest slopes next to it and has the most confined valley. Valkeajoki is the most meandering with the gentlest slopes next to it and the broadest valleys. Äkäsjoki has the smallest change in height per 100 meters. These findings comply well with the actual properties of the rivers examined in GIS. Kuerjoki is very narrow and confined in a steep canyon about 25 m deep from its mouth up for about 1 km which lowers the mean ER value. Äkäsjoki also has a large area where the channel is relatively confined in a 35 m deep canyon, although it also has a large open valley segment when nearing Valkeajoki from upstream. Valkeajoki lacks significant confined valleys.

The high mean GW site density (15.1; Table 2) and mean entrenchment ratio value of Valkeajoki (43.1; Table 8) seems to match the results of the Pearson correlation where higher entrenchment ratio values produce more discharge sites. The mean gradient value for Valkeajoki (0.37) was in between the values of Äkäsjoki and Kuerjoki. As all of these values are mean values, only low or high values really give some insight about the effects of the metrics to the GW site occurrences or densities. The mean GW site density of Äkäsjoki (5.7; Table 2) is quite low but the mean ER value of 13.4 (Table 8) is not particularly low or high so not much can be deduced about the effects of the metric on the site amounts. Kuerjoki has the lowest mean ER value (11.4) but a relatively high mean site density (11.1) which doesn't quite follow the available results.

6.3 Applicability of used methods

The UAV methods were suited, although laborious, for the small-scale areas in Hannukainen for precise mapping of GW discharge sites. If the persistence or stability of GW discharge sites was the target of interest, a multiple-campaign study should be conducted which would be more time-consuming and add much more data to process. At a larger scale, the sheer amount of image data and Pix4D data would take up much more space and the workload needed for the image processing would be heavy. Some GW discharge sites were not very easily classified, and an automated process would have been interesting to utilize. Although at this scale with such a small amount of discharge sites it wouldn't provide that much time savings.

The thermal profiles were a late add-on to this study, as after processing the TIR imagery I realized that there was no easy way of telling the river temperature from the images. Luckily thermal profiles are common in riverine studies and lots of examples were available. The profiles proved very informative and useful in assessing the changes in the streams although the profiles only covered the short distances studied with the UAV. The examination and interpretation was done manually so it was also time-consuming. Marking the diffuse seepage areas to the profiles was challenging as this discharge site type covers an area rather than a discrete spot. Evaluating the effect of the diffuse site to the stream temperature was hard and visibly non-existent in some cases.

The choosing of the usable landscape metrics was not the easiest task as the conditions in the study area are different than in the other similar studies. The metric calculation process was time-consuming and required a lot trial and error learning because the processes are not described in detail anywhere. The extensive manual and help available for ArcMap was irreplaceable. Time was saved also with the already existing 2012–2013 GW discharge site data. Partly automated processes also at this part of the study could save some time but e.g. some R or MATLAB skills would be required. The landscape metric calculation process as used in this study would be strenuous to replicate as it is. The predictability of GW discharge sites in a river using landscape metrics could work, if there was a more established method

for the whole process as for choosing, calculating and correlating the metrics. There should be some uniform metric values or metric combinations that would serve as example or comparison values that represent the features of the most probable locations for GW sites to occur in.

The General linear model used in the metric - discharge site correlation gave only a yes/no answer whether there was correlation or not. The diagrams made from the significant GLM results turned out to be useless as the variance of the ER data was too high and after conducting Pearson's two-variable correlations gradient didn't correlate significantly with the discharge sites. A more clear understanding of correlation methods could have helped in choosing better suited methods. The overall complexity of hydrogeological subsurface processes combined with the effects of geomorphology offered a very challenging platform for interpretations. The Spearman's correlation method used between the different metrics gave an indication of the strength and direction of the correlation, albeit the correlated data was in ranked form.

6.3.1 Uncertainties in the methods and interpretations

The absolute temperatures used for the UAV data display were based on only a few reference measurements and the places where the measurements were made weren't necessarily situated within the UAV imaging area, and Akas TIR was left without a reference temperature. The too low absolute temperature values of the Pix4D-generated TIFFs and the image edge temperature decline were caused by incorrect thermal camera parameters. Instructions about the parameters to be used with the cameras of the UAV and in Pix4D user interface were not yet clearly established. A portion of 20–40 meters of the image edges was practically unusable for discharge site identification because the temperature anomaly could be due to the distortion. Some datasets were collected in sunny weather and the resulting TIFFs are much harder to interpret as high temperature changes are caused by tree shadows and possible cold water discharges are blended in the shadows.

The 10-meter DEM had the highest resolution available of the whole study area. Two-meter resolution was also available from a part of the area but to ensure uniform methods only the 10-m resolution was used. The 10-m DEM elevation accuracy of 1.4 meters seems quite vague for small streams such as Valkeajoki. The 2-m DEM based on laser scanning has an elevation accuracy of 30 cm which would have allowed more precise morphological calculations.

The resolution restrictions of the DEM could have affected the gradient, slope and entrenchment ratio landscape metric values, especially gradient values that were extracted straight from the DEM. There were some minor negative values which means that the river would go uphill at some point. However if the negative values were replaced with zeros or 0.001 the data would have become biased as there would be an unusually large amount of these new values. With the negative values the data was more normal looking so the values were left as they were.

Slope metric values were calculated from areas on both sides of the river. However there were often differences between the sides so that one side was flat with lower slope values and the other side steep with higher slope values. If the river sides had been calculated separately, there might have been a more significant correlation between slope values and the discharge site occurrence. On the other hand, this would have required extra processing and the results would have been harder to combine with the other landscape metric results. The other metrics could not have been calculated on both sides of the river as sinuosity and gradient focus on the river itself. Entrenchment ratio needs to be measured from the whole river valley to get sensible results.

Many parameters used in the calculation of the entrenchment ratio were based on spatially measured values in GIS. River depth values were not readily available so estimates were used based on discharge rates, GIS data and visual observations made in the field. The valley edge estimation (as in flood-prone width) was quite challenging as the edges had to be at a height two times the river depth measured from the bottom of the valley and the depth values had to be hand-picked.

The lack of correlations between the GW discharge sites and sinuosity and slope could be caused by inaccuracies in the metric calculation process. Also the formation of GW discharge sites is such a complex hydrogeological process that the effect of one or two metrics in dozens of other mechanisms is hard to verify. The influential metrics according to the General Linear Model (entrenchment ratio and gradient) left a lot to interpret about the discharge site distributions. Also in the end only ER was the only metric that was influential in both GLM and Pearson's correlations. The availability of more precise surficial deposit data could have enabled the use of many other relevant landscape metrics, now left out.

7. CONCLUSIONS

UAV GW discharge sites were classified into four categories: spring, diffuse seepage, relict channel and tributary confluence plume. Temperature profiles were created to examine the temperature changes along the rivers and what could cause the fluxes. In most cases the GW discharge sites alone caused only possible minor fluxes to the temperature, the main focus being on the effects of the morphological features of the rivers. The GW sites in the UAV data occurred most often in meandering sections of the rivers. Channel widening occurred often with dropping temperatures and narrowing with warming temperatures. Also lower T were observed after meanders or between meanders. Higher confinement was observed to occur with lower temperatures.

Four landscape metrics were used in accordance with the 2012–2013 GW discharge data: channel sinuosity, gradient, terrain slope and entrenchment ratio (ER). ER and gradient gave statistically significant results indicating connections to the discharge site occurrences and counts in a General Linear Model. Low R^2 values measuring the accuracy of the model were attained suggesting that a large part of the variance in the data remains unexplained by the metrics. With Pearson correlation between two variables at a time, only ER had statistical significance with the discharge sites. There was a weak positive linear relationship between

ER and the discharge site occurrences and counts, which means that more open valleys are more prone to having an increased amount of GW discharge sites. As the correlation is weak, a large part of the effects on the discharge amounts come likely from other riverine processes. Gradient effects on the discharge sites were left unclear due to the lack significance in the second correlation. The results partly agree and partly differ from the few studies that used similar metrics.

The metrics correlate with each other moderately to weakly or not at all. When ER decreases, terrain slope and stream gradient increase and sinuosity decreases and vice versa. As used in this study, the use of landscape metrics to predict the locations of GW discharge sites would be time-consuming and the reliability of results would be hard to ensure. More established methods for choosing, calculating and correlating the metrics would help in the process. Also an inventory for metric values or value combinations representing the probable locations of GW discharge sites would prove very useful.

8. ACKNOWLEDGEMENTS

I would like to thank my thesis supervisors Kirsti Korkka-Niemi and Anne Rautio for their guidance and help during this process. Also special thanks to the geology students community in my university for being awesome and providing a place to feel comfortable at. Thanks to my friends at an immeasurable importance for being there with your smiles and shoulders and my family for understanding and keeping me afloat.

9. REFERENCES

Dugdale, S. J., Bergeron, N. E. and St-Hilaire, A. 2013. Temporal variability of thermal refuges and water temperature patterns in an Atlantic salmon river. Remote Sensing of the Environment 136, 358–373.

Dugdale, S. J., Bergeron, N. E. and St-Hilaire, A. 2015. Spatial distribution of thermal refuges analysed in relation to riverscape hydromorphology using airborne thermal infrared imagery. Remote Sensing of Environment 160, 43-55.

Ebersole, J. L., Liss, W. J. and Frissel, C. A. 2003a. Cold water patches in warm streams: physicochemical charasteristics and the influence of shading. Journal of the American Water Resources Association 39, 355–368.

Ebersole, J. L., Liss, W. J. and Frissel, C. A. 2003b. Thermal heterogeneity, stream channel morphology, and salmonid abundance in northeastern Oregon streams. Canadian Journal of Fisheries and Aquatic Sciences 60, 1266–1280.

Elliott, C. M. E. 2011. Geomorphic classification and evaluation of channel width and emergent sandbar habitat rations on the Lower Platte River, Nebraska. USGS Scientific investigations report 2011–5028.

Faye, E., Rebaudo, F., Yánez-Cajo, D., Cauvy-Fraunié, S. and Dangles, O. 2016. A toolbox for studying thermal heterogeneity across spatial scales: from unmanned aerial vehicle imagery to landscape metrics. Methods in Ecology and Evolution 7, 437-446.

Finnish Environment Institute. 2012. CORINE land cover map of Finland 1:100 000.

Geological Survey of Finland. 2014. Bedrock map of Finland 1:100 000.

Geological Survey of Finland. 2012. Superficial deposits of Finland 1:200 000.

Hannukainen mining 2017. Hannukainen mining Ltd. Page visited 10.9.2017. http://www.hannukainenmining.fi/hannukainen-mining/kaivoshistoria.html

HERTTA database, environmental information management system. Finnish Environmental Institute. Site visited 9.3.2017.

Hiltunen, A. 1982. The Precambrian geology and skarn iron ores of the Rautuvaara area, northern Finland. Geological Survey of Finland Bulletin 318.

Hirvas, H. 1991. Pleistocene stratigraphy of Finnish Lapland. Geological Survey of Finland Bulletin 354, 123 p.

Jonsson, B. and Jonsson N. 2009. A review of the likely effects of climate change on anadromous Atlantic salmon *Salmo salar* and brown trout *Salmo trutta*, with particular reference to water temperature and flow. Journal of Fish Biology 75, 2381–2447.

Kline, M., Alexander, C., Pomeroy, S., Cahoon, B. and Becker, L. 2004. Vermont stream geomorphic assessment phase 2 handbook: Rapid stream assessment, Field protocols. Vermont Agency of Natural Resources.

Korkka-Niemi, K., Kivimäki, A-L., Lahti, K., Nygård, M., Rautio, A., Salonen, V-P. and Pellikka, P. 2012. Observations on groundwater-surface water interactions at River Vantaa, Finland. Management of Environmental Quality 23, 222–231.

Kujansuu, R. 1967. On the deglaciation of western Finnish Lapland. Bulletin de la commission géologique de Finlande 232, 1–98.

Lunkka, J. P., Sarala, P. and Gibbard, P. L. 2015. The Rautuvaara section, western Finnish Lapland, revisited – new age constraints indicate a complex Scandinavian Ice Sheet history in northern Fennoscandia during the Weichselian Stage. Boreas 44, 68–80.

Monk, W. A., Wilbur, N. M., Curry, R. A., Gagnon, R. and Faux, R. N. 2013. Linking landscape variables to cold water refugia in rivers. Journal of Environmental Management 118, 170–176.

Niiranen, T., Poutiainen, M. and Mänttäri, I. 2007. Geology, geochemistry, fluid inclusion charasteristics, and U-Pb age studies on iron oxide-Cu-Au deposits in the Kolari region, northern Finland. Ore Geology Reviews 30, 75–105.

Ozaki, V. 1988. Geomorphic and hydrologic conditions for cold pool formation on Redwood National Park. Technical report 24, Arcata, California.

Pirinen P., Simola H., Aalto J., Kaukoranta J-P., Karlsson P. and Ruuhela R. 2012. Climatological statistics of Finland 1981–2010. Finnish meteorological institute reports 2012:1.

Pix4D Support 2016. Pix4D support, frequently asked questions page. Page visited 9.10.2016. https://support.pix4d.com/hc/en-us/articles/360000173463-Processing-thermal-images#label5

Pöyry Finland Ltd. 2010. Northland mines Oy – Ympäristövaikutusten arviointiohjelma.

Ranta, E., Rita, H. and Kouki, J. 2012. Biometria - Tilastotiedettä ekologeille. Gaudeamus Helsinki University Press, Helsinki, 10th edition, 567 p.

Rautio, A., Kivimäki,A-L., Korkka-Niemi, K., Nygård, M., Salonen, V-P., Lahti, K. and Vahtera, H. 2015. Hydrology and Earth System Sciences 19, 3015–3032.

Rautio, A. B., Korkka-Niemi, K. I. and Salonen, V-P. 2017. Thermal infrared remote sensing in assessing groundwater and surface-water resources related to Hannukainen mining development site, northern Finland. Hydrogeology Journal 26, 163–183.

Rosgen, D., L. 1994. A classification of natural rivers. Catena 22, 169–199.

Rosenberry, D.O. and LaBaugh, J.W., 2008. Field Techniques for Estimating Water Fluxes Between Surface Water and Ground Water. U.S. Geological Survey Techniques and Methods 4–D2, 128 p.

Salonen, V-P., Moreau, J., Hyttinen, O. and Eskola, K. O. 2014a. Mid-Weichselian interstadial in Kolari, western Finnish Lapland. Boreas 43, 627–638.

Salonen, V-P., Korkka-Niemi, K., Moreau, J. and Rautio, A. 2014b. Kaivokset ja vesi – esimerkkinä Hannukaisen hanke. Geologi 66, 8–19.

Stanford, J. A. and Ward, J. V. 1993. An ecosystem perspective of alluvial rivers: connectivity and the hyporheic corridor. Journal of the North American Benthological Society 12, 48–60.

Torgensen C. E., Price, D. M., Hiram, W. L. and McIntosh, B. A. 1999. Multiscale thermal refugia and stream habitat associations of Chinook salmon in Northeastern Oregon. Ecological Applications 9, 301–319.

Torgensen, C. E., Faux, R. N., McIntosh, B. A., Poage, N. J. and Norton, D. J. 2001. Airborne thermal remote sensing for water temperature assessment in rivers and streams. Remote Sensing of the Environment 76, 386–398.

Torgensen, C. E., Ebersole, J. L. and Keenan, D. M. 2012. Primer for identifying cold-water refuges to protect and restore thermal diversity in riverine landscapes. U.S. Environmental Protection Agency, Seattle, Washington, 91 p.

Vähä, V., Romakkaniemi, A., Pulkkinen, K., Ankkuriniemi, M., Keinänen, M., Lilja, J. ja Leminen, M. 2014. Lohi- ja meritaimenkantojen seuranta Tornionjoen vesistössä vuonna 2013. Riista- ja kalatalous – Tutkimuksia ja selvityksiä 2/2014, 28 p.

Wawrzyniak, V., Piégay, H., Allemand, P., Vaudor, L., Goma, R. and Grandjean, P. 2016. Effects of geomorphology and groundwater level on the spatio-temporal variability of riverine cold water patches assessed using thermal infrared (TIR) remote sensing. Remote Sensing of the Environment 175, 337–348.